Unveiling the role of local metabolic constraints on the structure and activity of spiking neural networks

Ismael Jaras[1,2*], Marcos E. Orchard[1], Pedro E. Maldonado[2,4], Rodrigo C. Vergara[3,4*]

1 Department of Electrical Engineering, Faculty of Mathematical and Physical Sciences, University of Chile, Santiago, Chile
2 Neurosystems Laboratory, Biomedical Neuroscience Institute, Faculty of Medicine, University of Chile, Santiago, Chile
3 Facultad de Psicología y Humanidades, Universidad San Sebastián, Valdivia, Chile
4 Centro Nacional de Inteligencia Artificial CENIA, Chile

* ismael.jaras@ing.uchile.cl * rodrigo.vergara@uss.cl

Abstract

Understanding the intricate interplay between neural dynamics and metabolic constraints is crucial for unraveling the mysteries of the brain. Despite the significance of this relationship, specific details concerning the impact of metabolism on neuronal dynamics and neural network architecture remain elusive, creating a notable gap in the existing literature. This study employs an energy-dependent neuron and plasticity model to analyze the role of local metabolic constraints in shaping both the dynamics and structure of Spiking Neural Networks (SNN). Specifically, an energy-dependent version of the leaky integrate-and-fire model is utilized, along with a three-factor learning rule that incorporates postsynaptic available energy as the third factor. These models allow for fine-tuning sensitivity in the presence of energy imbalances. Analytical expressions predicting the network's activity and structure are derived, and a fixed-point analysis reveals the emergence of attractor states characterized by neuronal and synaptic sensitivity to energy imbalances. Analytical findings are validated through numerical simulations using an excitatory-inhibitory balanced network. Furthermore, these simulations enable the study of SNN activity and structure under conditions simulating metabolic impairment. In conclusion, by employing energy-dependent models with adjustable sensitivity to energy imbalances, our study advances the understanding of how metabolic constraints shape SNN dynamics and structure. Moreover, in light of compelling evidence linking neuronal metabolic impairment to neurodegenerative diseases, the incorporation of local metabolic constraints into the investigation of neuronal network structure and activity opens an intriguing avenue for inspiring the development of therapeutic interventions.

Introduction

Neural tissue consumes a higher amount of energy resources compared to other somatic tissues [1], where electric activity corresponds to 92% of neuron expenses [2]. This amount of resource consumption is not trivial as neurons are extremely sensitive to resource deprivation, particularly to decrease of oxygen and glucose levels on blood or cerebrospinal fluid (CSF) [3]. Even more, many neurodegenerative diseases, such as Parkinson's disease, Leigh, amyotrophic lateral sclerosis (ALS), and Alzheimer's disease

have been proposed to occur due to energy management impairment [4–9]. Despite the recognized relevance of energy management in the nervous system [10, 11], energy management is rarely considered as a relevant factor in neuroscience and in neural modeling.

Energy management also appears relevant in common behavioral activities. Neural activity elicits local increases in blood flow (neurovascular coupling), glucose uptake, and oxygen consumption [12], being this same energy management mechanism the one used in fMRI to map behavior into the brain [13]. As such, fMRI evidence could also be interpreted as a correlate of behavior with energy management in neural tissue. However, the energy management of active neurons is even more finely tuned. For instance, neurons outsource glycolytic activity to astrocytes leaving energy levels fairly constant during time [14]. Besides the energy substrates given by astrocytes during neuronal activity, neurons are provided with intrinsic mechanisms that buffer ATP levels. Accordingly, neuron mitochondria raise ATP synthesis in response to an increment in synaptic stimuli [9, 15–18]. Together, these arguments present robust evidence that supports the importance of energy administration for maintaining the brain's proper function, thereby leading to the development of modeling strategies that account for metabolic dynamics.

Attempting to establish the significance of energy management as a pivotal factor influencing neural systems, the Energy Homeostasis Principle (EHP) was introduced in [10, 11]. The rationale behind this principle posits that neurons, in meeting their metabolic needs, inadvertently address behavioral challenges as an epiphenomenon. A key assertion of the EHP is that energy management profoundly influences neural network dynamics. While neurons lack direct control over presynaptic stimulation, they exert influence over the "weight" or strength of such activity. Consequently, the core hypothesis derived from the EHP posits that energy management significantly shapes synaptic weights, consequently impacting the broader dynamics of neural systems.

While the Energy Homeostasis Principle (EHP) has made strides in addressing certain gaps in understanding, a comprehensive grasp of the effects of local energy constraints at a network level remains elusive. To advance our comprehension of the impact of metabolic constraints on the brain, an effective strategy involves formalizing neuronal and synaptic models. This formalization should encompass experimentally observed energy dependencies, affording the opportunity to analytically scrutinize the implications of metabolic constraints as well as simulate their effects. This work fills the gap by committing to the previous approach. Here we create an energy-dependent Spike-timing-dependent plasticity rule and, jointly with a previously introduced energy-dependent neuronal model [19], we study the role of local metabolic constraints on the structure and activity of spiking neural networks, particularly in Excitatory-Inhibitory (E-I) balanced networks. Our exploration employs two complementary methods to assess the impact of metabolic constraints at the network level. Initially, we conduct a mathematical analysis to understand the consequences of incorporating energy dependencies into both neurons and synapses. Subsequently, we undertake simulations to further analyze the effects of metabolic constraints, providing a basis for comparison against the analytical results.

Through our mathematical analysis, we find the conditions under which the network converges toward a fixed point. Then, we compare theoretical predictions with numerical simulations, observing a good agreement between both. Regarding different simulation cases, we divide the experiments into three main scenarios. Firstly, we study the dynamics and structure of the E-I balanced networks focusing solely on synaptic sensitivity to energy imbalances. Following this, we extend our simulations to include neuronal sensitivity to energy imbalances. Finally, motivated by the evidence linking neurodegenerative diseases to metabolic impairments, we investigate the effect of

neuronal impaired metabolic productions on the dynamics and structure of the network.

Basically, realizing how crucial energy management is for shaping neural systems, this study aims to advance our understanding of how local metabolic constraints influence the structure and activity of spiking neural networks. To achieve this, we introduce a novel energy-dependent plasticity rule and investigate the impact of local metabolic constraints through both analytical methods and numerical simulations.

Materials and methods

We want to study and understand the impact of metabolic constraints at the network level. One approach to accomplish this is by including energy dependencies at the neuronal and synaptic levels. We will start by introducing the neuronal model that we are using:

Energy dependent Leaky integrate-and-fire (EDLIF)

The Leaky integrate-and-fire (LIF) model is a single-compartment model describing the subthreshold dynamics of the neuron membrane potential. Despite its simplicity, the LIF model it is widely used for modeling neuronal dynamics. The LIF model does not take into account neuronal energetics affecting his dynamics, however, ultimately, the function of the neuron rests on its ability to balance its energy expenditure and production. Within this balance, the sodium-potassium pump is a key actor, considering that it relies on available ATP to restore the resting potential allowing action potentials to occur [20]. Consequently, neuronal behavior depends on the adequate balance between energy production and expenditure. The main objective of the EDLIF [19] model is to include the energy dependence in the neuronal dynamics while maintaining the LIF model's simplicity. To accomplish that, the EDLIF model makes the neuronal behavior explicitly dependent on the available neuronal energy through the energy-dependent partial repolarization mechanism.

As in the LIF model, in the EDLIF model the membrane's voltage of the neuron is described as follows:

$$C_m \frac{dv(t)}{dt} = -g_{leak}(v(t) - v_{rest}) + I(t), \tag{1}$$

where C_m is the membrane capacitance, v_{rest} the equilibrium potential of the leak channel, and g_{leak} is the conductance associated with the current leakage. Unlike the LIF model, in the EDLIF model the reset potential after an action potential occurs is metabolically dependent. This dependency is achieved by the inclusion of a partial repolarization mechanism [21], which works by resetting the potential of the capacitor to $v_{reset} = \beta v_{th}$ after an action potential occurs, where v_{th} is the firing threshold and β is called the reset parameter. In the EDLIF model, the reset parameter (β) depends on ATP as follows:

$$\beta(A(t)) = 1 + \alpha\left(2 - \frac{2}{1 + e^{-\frac{A_H - A(t)}{A_H}\gamma}}\right), \tag{2}$$

where $\alpha = v_{rest}/v_{th} - 1$. This relationship represents the membrane repolarization voltage values after an action potential occurs as a function of the available ATP in the neuron. Given that the precise curve of the repolarization membrane voltage depending on ATP is unknown, a sensitivity parameter γ is introduced. This parameter provides the flexibility to adjust the intensity at which the repolarization membrane voltage value is affected by ATP level changes.

When a constant suprathreshold stimuli ($I_{inj} = I_0 > v_{th} g_{leak}$) is applied to the neuron's model with initial condition $v_m(t = 0) = v_{reset}(A)$, the membrane's potential satisfies the following trajectory:

$$v_m(t) = v_\infty[1 - e^{-t/\tau_m}] + v_{reset}(A)e^{-t/\tau_m}, \tag{3}$$

where $v_\infty = (I_0/g_{leak} + v_{rest})$. The time it takes for a spike to be generated (*i.e.*, the interspike interval, s_0) is obtained by imposing $v_m(s_0) = v_{th}$ [22]:

$$s_0(A) = \tau_m ln\Big[\frac{v_\infty - v_{reset}(A)}{v_\infty - V_{th}}\Big]. \tag{4}$$

Therefore, the corresponding ATP-dependent spiking-rate $\lambda(A)$ is described by the following equation:

$$\lambda(A) = (\tau_{ref} + s_0)^{-1}. \tag{5}$$

In accordance with Eqn (5), Fig. 1 shows how the neuron's firing rate response to an injected constant current changes when the neuronal sensitivity to energy imbalances (γ) is modified.

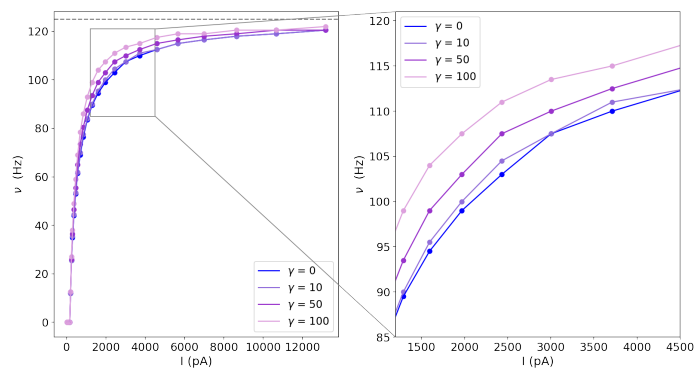

Fig 1. Current-frequency mapping for neurons with different γ sensitivity. The current-frequency mapping depends on the neuronal sensitivity to energy imbalances. If γ is higher the neuron's firing rate saturates before (with a smaller current) in contrast to a neuron with lower neuronal sensitivity to energy imbalances.

Neuronal ATP dynamics

In the EDLIF model, the ATP dynamics are characterized by considering two processes: those that supply ATP to the neuron ($A_s(t)$), and those that consume ATP ($A_c(t)$). The available ATP in the neuron ($A(t)$) can be formalized as follows [10]:

$$\frac{dA(t)}{dt} = A_s(t) - A_c(t), \tag{6}$$

and the neuron's homeostatic mechanisms attempt to keep ATP levels close to the homeostatic ATP level (A_H). The ATP production dynamics is mathematically formalized by Eqn. (7). Thus, ATP production depends on the actual ATP level with respect to a homeostatic one ($K(A_H - A(t))$) and a basal production term (A_B) accounting for resting potential and housekeeping activities:

$$A_s(t) = K(A_H - A(t)) + A_B, \tag{7}$$

where the parameter K ($(1/ms)$ units) is the rate at which ATP is produced.

Regarding energy consumption, we consider four energy-consuming activities in this study. Namely, the energy related to the neuron's housekeeping activities E_{hk}, the energy associated with maintaining the resting potential E_{rp}, the total energy expended by the neuron's action potentials E_{ap}, and the total energy associated with receiving postsynaptic potentials due to a presynaptic neighbor neurons having action potentials (E_{syn}). Both rate consumptions E_{hk} and E_{rp} are measured in energy per time units. On the other hand, both consumption activities E_{ap} and E_{syn} refer to the total amount of energy consumed by those activities. To obtain the corresponding rate consumption for E_{ap} and E_{syn} we use temporal kernels. In this manner, the amount of energy expended per time unit associated with action potentials (or postsynaptic potentials) is described as $A_{ap}(t) = E_{ap}\varepsilon_{ap}(t)$ (or $A_{syn}(t) = E_{syn}\varepsilon_{syn}(t)$), where $\varepsilon_x(\cdot)$ is the kernel associated to the process x and $\int_0^\infty \varepsilon_x(t)dt = 1$.

Originally, in the EDLIF model the production and consumption of ATP is measured in mM/ms, while the available ATP $A(t)$ is measured in mM. However, experimentally, it is difficult to precisely measure ATP concentrations in single neurons or populations. To overcome this difficulty and to define a more general framework, here we will use percentage units to quantify available energy ($A(t)$), homeostatic energy ($A_H = 100\%$), and activity-related energy consumption such as action potential energy consumption (E_{ap}), house-keeping (E_{hk}), resting potential (E_{rp}), and postsynaptic energy consumption (E_{syn}).

Static synapses and energy consumption in the neuron

To understand in detail the energy perturbations induced by presynaptic neurons in postsynaptic energy levels through synapses, let us analyze the neuron's energy dynamics when several presynaptic neurons are connected to it. In a network, each neuron's energy evolves following Eqn. (6), where $A_s = K(A_H - A) + A_B$, and the energy consumption A_c can be divided into the following terms:

$$A_c(t) = A_B + A_{ap}(t) + A_{syn}(t), \tag{8}$$

where A_B is the basal consumption accounting for resting potential and housekeeping activities, A_{ap} is the energy consumption accounting for the neuron action potentials, and A_{syn} is the energy consumption related to receiving action potentials from other neurons through the synapses. Please realize that $A_{ap}(t)$ ($A_{syn}(t)$) is different than E_{ap} (E_{syn}). The former is the action potential (postsynaptic) energy consumption through time, and the latter is the total amount of energy related to that activity. Thus, A_{ap} (A_{syn}) is obtained using E_{ap} (E_{syn}) and a kernel function $\varepsilon(\cdot)$, which describes how the total energy consumption is expended through time.

The solution to Eqn. (6) with an arbitrary energy consumption $A_c(t)$ is described by Eqn. (9):

$$A(t) = A_H - \int_0^t e^{-(t-t')/\tau_A} A_c(t')dt', \tag{9}$$

where $K = 1/\tau_A$ is the rate at which ATP can be produced in the neuron (see Eqn. (7)). Eqn. (9) can be found using the impulse response of the system described by Eqn. (6), together with the superposition principle.

Now we will describe how presynaptic activity affects postsynaptic available energy levels. For one presynaptic action potential propagating through a synapse with fixed strength w, the synaptic consumption on the postsynaptic neuron can be described by:

$$A_{syn}(t) = E_{syn}\bar{w}\Theta(t - t_s)\varepsilon_{syn}(t - t_s), \tag{10}$$

where $\Theta(\cdot)$ denotes the Heaviside step function, E_{syn} is the total energy expended for an incoming presynaptic action potential, $\bar{w}$ is the absolute value of the normalized synaptic strength ($\bar{w} = |w/w_{max}|$, where w_{max} is the maximum allowed weight strength) and $\varepsilon_{syn}(t)$ is a kernel describing how the synaptic energy expenditure is expended through time ($\int_0^\infty \Theta(t)\varepsilon_{syn}(t)dt = 1$). If we choose a kernel that can be linearly summed up, then the synaptic energy expenditure in the postsynaptic neuron due to several presynaptic cells with their respective spike times is:

$$A_{syn}(t) = E_{syn} \sum_{synapse\ k} \sum_{spike\ s} \bar{w}_k \Theta(t - t_s)\varepsilon_{syn}(t - t_s). \tag{11}$$

Similarly, for each action potential in the postsynaptic neuron, the energy expenditure can be described by:

$$A_{ap}(t) = E_{ap}\Theta(t - t_s)\varepsilon_{ap}(t - t_s), \tag{12}$$

where E_{ap} is the energy expenditure related to one action potential and ε_{ap} is analogous to ε_{syn}, but for the postsynaptic action potentials ($\int_0^\infty \Theta(t)\varepsilon_{ap}(t)dt = 1$). If ε_{ap} can be linearly summed up, then Eqn. (12) reads:

$$A_{ap}(t) = E_{ap} \sum_{spike\ s} \Theta(t - t_s)\varepsilon_{ap}(t - t_s). \tag{13}$$

For finding closed-form expressions for the available energy in the postsynaptic neuron, it is possible to define ε_{ap} and ε_{syn} kernels and plugin Eqns. (11) and (13) into Eqn. (6). In particular, if exponential kernels are used for ε_{ap} and ε_{syn}, Eqn. (11) reads:

$$A_{syn}(t) = \sum_{synapse\ k} \sum_{spike\ s} \frac{\bar{w}_k E^k_{syn}}{\tau^{A,k}_{syn}} \Theta(t - t_s) e^{-(t-t_s)/\tau^{A,k}_{syn}}, \tag{14}$$

where $\tau^{A,k}_{syn}$ is the energy time constant of the kth synapse and describes how *fast* is the change in the postsynaptic neuron's energy given the incoming action potential through the kth synapse. Note that if $w_k = w_{max}$ the total energy consumption in the postsynaptic neuron produced by the presynaptic neuron sending one action potential through synapse kth is E^k_{syn}. Thus, Eqn. (14) guarantees that for the maximum allowed synaptic weight, the total energy consumption perceived by the postsynaptic neuron is exactly E^k_{syn} and a fraction ($|w_k/w_{max}|$) of E^k_{syn} otherwise. Similarly, using an exponential kernel, Eqn. (13) can be expressed as:

$$A_{ap}(t) = \Theta(t - t_s)\frac{E_{ap}}{\tau_{ap}} e^{-(t-t_s)/\tau_{ap}}, \tag{15}$$

where τ_{ap} is the time constant defining how *fast* is E_{ap} expended through time. Eqn. (15) guaranties that the neuron will consume a total amount of E_{ap} for each action potential.

Therefore, plugin Eqns. (15) and (14) into Eqn. (9), we have a closed-form expression for the neuron's energy dynamics under exponential kernels (ε_{ap} and ε_{syn}) for energy consumption:

$$\begin{aligned} A(t) =& A_H - \overbrace{\frac{E_{ap}\tau_A}{\tau_A - \tau_{ap}} \sum_{spike\ s} \Theta(t - t_s)[e^{-(t-t_s)/\tau_A} - e^{-(t-t_s)/\tau_{ap}}]}^{A_{ap}(t)} \\ & - \underbrace{\sum_{synapse\ k} \sum_{spike\ f} \frac{E^k_{syn}\bar{w}_k\tau_A}{(\tau_A - \tau^{A,k}_{syn})}[e^{-(t-t_f)/\tau_A} - e^{-(t-t_f)/\tau^{A,k}_{syn}}]}_{A_{syn}(t)}. \end{aligned} \tag{16}$$

Eqn. (16) describes the energy dynamics of a single neuron within a network, given all incoming synapses strengths and spike-times. Thus, it allows to precisely quantify and analyze the energy dynamics of each neuron within a network with arbitrary architecture.

Energy dependent Spike-timing-dependent plasticity

We aim to investigate how local energy limitations influence network attributes. While having an energy-dependent single-neuron model is crucial, it's not the only consideration. We must also factor in the metabolic impact on synapses. The energy administration of the neuron is essential for its adequate operation, and considering the significant effect of these restrictions on synaptic activity [8, 9, 23, 24], the need to have synaptic transmission rules that depend on the energy management of the cell naturally emerges.

Energy dependent Spike-timing-dependent plasticity model

Here we leverage previously defined plasticity models to introduce an energy-dependent synaptic plasticity rule. Particularly, we introduced an energy-dependent plasticity rule for synaptic strength. We follow the formalization of STDP introduced in [25]:

$$\Delta w = \begin{cases} \lambda f_+(w) K(\Delta t), & \text{if } \Delta t > 0. \\ -\lambda f_-(w) K(\Delta t), & \text{if } \Delta t \leq 0, \end{cases} \tag{17}$$

where the synaptic efficacy w is normalized to $[0, 1]$. The learning rate λ $(0 < \lambda \ll 1)$ scales the magnitude of the individual weight change, $K(\cdot)$ is a temporal filter $K(x) = e^{-\|x\|/\tau_{stdp}}$, and $f_\pm(\cdot)$ is defined as follows:

$$f_+(w) = (1 - w)^{\mu_+} \text{ and } f_-(w) = \alpha w^{\mu_-}, \tag{18}$$

with $\alpha > 0$ accounting for the asymmetry between the scales of potentiation and depression.

Our energy-dependent plasticity rule is inspired by the findings shown in [26]. We focus on the fact that plasticity, in particular Long-Term Potentiation (LTP), depends on metabolism. Specifically, when glycolysis is pharmacologically inhibited (thus ATP production from glucose is inhibited), LTP is suppressed [26]. Therefore, our energy-dependent STDP rule should suppress LTP when there is a low energy level. Following this observation, we proceed to extend Eqn. (17) to account for energetics, while keeping in mind that this is a practical simplification of a more complex biological phenomena, but which allows deepening the understanding of metabolism and plasticity interactions, and its impact on neural network dynamics.

To account for energetics in STDP, it is possible to extend $f_+(w)$ in Eqn. (18) to include the energy level A of the postsynaptic neuron, obtaining $f_+(w, A)$. There are several ways to mathematically formalize the inclusion of postsynaptic energy level in $f_+(w)$, but we follow a similar rationale as the one used in EDLIF neuron, namely, we want energy-dependent STDP to be *sensitive* to energy imbalance. Hence, we can investigate not only how energy affects STPD, but also how energy imbalance affects STDP given a certain level of *energy imbalance sensitivity* in that synapse's plasticity. Using the rationale mentioned above we extend $f_+(w)$ to $f_+(w, A)$ as follows:

$$f_+(w, A) = f_+(w) e^{-\eta \frac{A_H - A}{A_H}}, \tag{19}$$

where η is the sensitivity of the synapse's plasticity to energy imbalances, A_H is the homeostatic energy level, and A is the postsynaptic energy level. STDP effects can be

thought as a change in postsynaptic receptor density. Given that the postsynaptic neuron has to modify its receptor's density, their energy level is affecting receptor density modifications, and we do not need to consider presynaptic energy level. Please note that if the synapse is not sensitive to energy imbalances (*i.e.,* $\eta = 0$), then we recover the original STDP rule.

The postsynaptic energy level can be interpreted as a plasticity moderator. Thus, our energy-dependent STDP rule is a special case of a three-factor learning rule, with postsynaptic available energy A as modulator, as shown in Fig. 2. For the depression

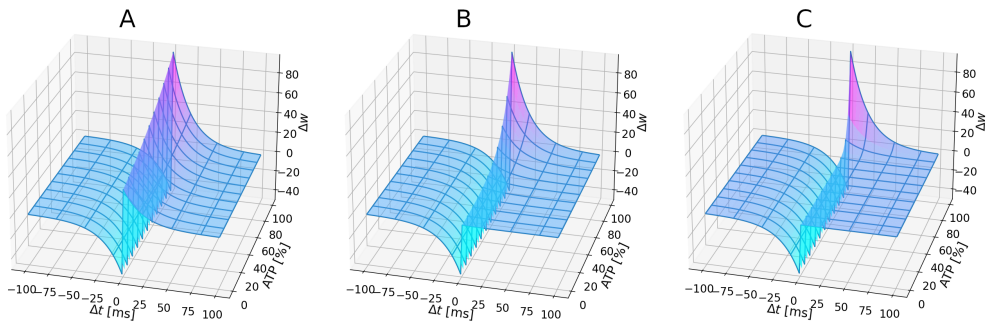

Fig 2. Energy-dependent STDP. Weight potentiation depends on postsynaptic available energy A. If energy $A = A_H$, the original STDP rule is recovered, while for $\eta = 0$ the synapse's plasticity is insensitive to energy imbalance, thus weight update only depends on spike-timing differences (Δt). If the postsynaptic available energy decreases, potentiation is suppressed and potentiation suppression depends on the sensitivity parameter η. (A) sensitivity $\eta = 1$, (B) sensitivity $\eta = 5$, (C) sensitivity $\eta = 20$.

updating function $f_-(w)$ we keep the original formulation ($f_-(w) = \alpha w^{\mu_-}$, see Eqn. (18)) because we do not have conclusive evidence justifying the depression dependence on postsynaptic available energy. However, energy may be also affecting depression.

Plugging Eqn. (19) into Eqn. (17), it is possible to describe weight's update accounting for pre- and postsynaptic spike-time and postsynaptic energy level:

$$\Delta w = \begin{cases} \lambda f_+(w, A) e^{-\Delta t/\tau_+}, & \text{if } \Delta t > 0. \\ -\lambda f_-(w) e^{\Delta t/\tau_-}, & \text{if } \Delta t \leq 0. \end{cases} \tag{20}$$

In principle, Eqn. (20) allows to include weight w dependencies in the updating rule if $\mu_\pm > 0$. In those cases, the updating rule is called a multiplicative rule, while if $\mu_\pm = 0$ the updating rule is additive, because weight update is independent of the current weight value. Multiplicative rules generate uni-modal weight distributions, while additive rules generates bi-modal weight distributions [25]. Bi-modal weights distributions are observed in biology, and because mathematical tractability of STDP additive rules is easier than multiplicative ones, in what follows we decided to focus on additive update rule for weights update ($\mu_\pm = 0$); however, there is also significant biological evidence supporting multiplicative STDP as well. For this reason, we define Eqn. (20) in a general form, allowing the exploration of multiplicative energy-dependent STDP in future works.

Network model

There is biological evidence suggesting the existence of excitatory-inhibitory (E-I) balanced networks in different parts of the brain, such as the CA3 region of the

hippocampus, basal ganglia, and the primary visual cortex [27]. Thus, E-I balanced networks appear as a suitable model to explore neural networks' dynamics and structure. However, in general, energy or metabolic constraints are not considered when simulating and studying E-I balanced networks.

To mathematically describe an E-I balanced network (Fig. 3) with n_{ex} excitatory and n_{in} inhibitory neurons, we introduce the network's weight matrix $\mathbf{w}$ of $(n_{ex} + n_{in}) \times (n_{ex} + n_{in})$ dimension:

$$\mathbf{w} = \left(\begin{array}{c|c} \mathbf{w^{ex\to ex}} & \mathbf{w^{ex\to in}} \\ \hline \mathbf{w^{in\to ex}} & \mathbf{w^{in\to in}} \end{array}\right),$$

where the i, j element of $\mathbf{w}$ correspond to the synapse from the ith presynaptic neuron to the jth postsynaptic neuron. $\mathbf{w^{ex\to ex}}$ is the $n_{ex} \times n_{ex}$ matrix containing all the excitatory-excitatory connections, $\mathbf{w^{ex\to in}}$ is the $n_{ex} \times n_{in}$ matrix containing all the excitatory-inhibitory connections, $\mathbf{w^{in\to ex}}$ is the $n_{in} \times n_{ex}$ matrix containing all the inhibitory-excitatory connections, and $\mathbf{w^{in\to in}}$ is the $n_{in} \times n_{in}$ matrix containing all the inhibitory-inhibitory connections. Because both LTP and LTD depended on the activation of NMDA receptors and are absent in cases in which the postsynaptic neurons were GABAergic in nature [28], only excitatory-excitatory ($\mathbf{w^{ex\to ex}}$) connections are plastic in our E-I network. The mean firing rate of each neuron in the $[t, t + T]$ interval, is described by the $(n_{ex} + n_{in}) \times 1$ vector $\bar{\nu}_{\mathbf{t}}$:

$$\bar{\nu}_{\mathbf{t}} = \left(\frac{\bar{\nu}^{\mathbf{ex}}_{\mathbf{t}}}{\bar{\nu}^{\mathbf{in}}_{\mathbf{t}}}\right),$$

where $\bar{\nu}^{\mathbf{ex}}_{\mathbf{t}}$ is the $n_{ex} \times 1$ dimension vector containing the excitatory mean firing rate, whereas $\bar{\nu}^{\mathbf{in}}_{\mathbf{t}}$ contains the inhibitory mean firing rates in a $n_{in} \times 1$ dimension vector.

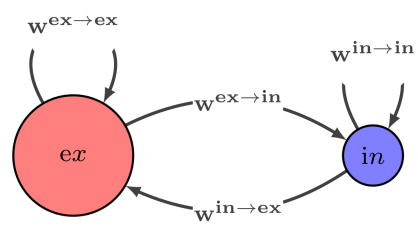

Fig 3. Excitatory-inhibitory balanced network.
The network is composed of excitatory and inhibitory neuronal populations, with excitatory-excitatory $\mathbf{w^{ex\to ex}}$, excitatory-inhibitory $\mathbf{w^{ex\to in}}$, inhibitory-excitatory $\mathbf{w^{in\to ex}}$ and inhibitory-inhibitory $\mathbf{w^{in\to in}}$ connections. All connections are static, except the excitatory-excitatory connections, which evolve following the Energy-Dependent STDP plasticity rule.

Network's firing-rate

To improve our analytical understanding of the E-I balanced network, it is practical to have an approximation of the network's firing rate ν, quantifying each neuron firing rate. In principle, using the LIF model (or the EDLIF model with no energy sensitivity to energy imbalances, *i.e.,* $\gamma = 0$) and knowing the model's parameters, the firing rate of a neuron excited by a constant current can be easily calculated. In a more general way, the firing rate of a neuron can be calculated by defining a function $\phi : \mathbb{R} \to \mathbb{R}$, mapping stimulation current to firing rate. If the neuron is insensitive to energy

imbalance (*i.e.*, $\gamma = 0$) and is excited with a supra-threshold current I, then the function $\phi(\cdot)$ can be found utilizing Eqn. (21):

$$T_n = \tau_{ref} + \tau_m \ln\Big(\frac{v_\infty - v_{reset}}{v_\infty - v_{th}}\Big), \tag{21}$$

where τ_{ref} is the neuron's refractory period, $\tau_m = C_m/g_{leak}$ is the neuron's time constant, and $v_\infty = I/g_{leak} + v_{reset}$. In this case, $\nu = T_n^{-1} = \phi(I)$, where I is the constant incoming current to the neuron. Thus, the firing rate of each neuron under a constant current stimulation can be calculated knowing the neuron's parameters as well as the incoming constant current and the $\phi(\cdot)$ function, which is monotonically increasing in I (if $I \leq I^{'} \Rightarrow \phi(I) \leq \phi(I^{'})$. Thus, if the incoming current I increases, the firing rate of the neuron increases or stays constant). Therefore, if we can approximate the mean incoming current $\bar{I}_t$ to a neuron in a small time-window, it is possible to approximate the neuron's firing rate $\bar{\nu}_t \approx \phi(\bar{I}_t)$, where $\bar{x}_t = T^{-1}\int_t^{t+T} x(t')dt'$. Hence, to approximate each neuron's firing rate, let us approximate the mean incoming current $\bar{I}_t$ to each neuron:

$$\begin{aligned}\bar{I}_t =& \frac{1}{T}\int_t^{t+T} I(t')dt' \\ =& \frac{1}{T}\int_t^{t+T} I_{stim} + \sum_{synapses\ k}\sum_{spike\ s} w_k \varepsilon_k(t'-t_s)dt'.\end{aligned} \tag{22}$$

Therefore, the mean incoming current to a neuron is the mean incoming synaptic current, plus the constant external incoming stimulation current I_{stim} injected into the neuron. Eqn. (22) describes the mean incoming current to a neuron utilizing an $\varepsilon_k(\cdot)$ interaction kernel. If we use a delta Dirac interaction kernel (*i.e.*, $\varepsilon_k(\cdot) = \delta(\cdot)$), Eqn. (22) reads:

$$\begin{aligned}\bar{I}_t =& I_{stim} + \sum_{synapse\ k} w_k \underbrace{\frac{1}{T}\int_t^{t+T}\sum_{spike\ s}\delta(t'-t_s)dt'}_{\bar{\nu}_t^k} \\ =& I_{stim} + \sum_{synapse\ k} w_k \bar{\nu}_t^k.\end{aligned} \tag{23}$$

If we define the constant incoming stimulation current to each neuron as the $(n_{ex}+n_{in})\times 1$ dimension vector $\mathbf{I_{stim}^\top} = [(\mathbf{I_{stim}^{ex}})^\top, (\mathbf{I_{stim}^{in}})^\top]^\top$, and the mean incoming synaptic current as the $(n_{ex}+n_{in})\times 1$ dimension vector $\bar{\mathbf{I}}_\mathbf{t}^\top = [(\bar{\mathbf{I}}_\mathbf{t}^\mathbf{ex})^\top, (\bar{\mathbf{I}}_\mathbf{t}^\mathbf{in})^\top]^\top$, Eqn. (23) can be expressed in matrix form as follows:

$$\bar{\mathbf{I}}_\mathbf{t}^\top = \mathbf{I_{stim}^\top} + \bar{\nu}_\mathbf{t}^\top \bar{\mathbf{w}}_\mathbf{t}. \tag{24}$$

It is possible to apply $\phi(\cdot)$ point-wise to obtain the approximated network's firing rate:

$$\begin{aligned}\bar{\nu}_\mathbf{t}^\top \approx& \phi(\bar{\mathbf{I}}_\mathbf{t}^\top) \\ =& \phi(\mathbf{I_{stim}^\top} + \bar{\nu}_\mathbf{t}^\top \bar{\mathbf{w}}_\mathbf{t}).\end{aligned} \tag{25}$$

Eqn. (25) imposes a current-frequency constraint on the network. In general, $\phi(\cdot)$ defines a nonlinear relationship between incoming current and the neuron's firing rate. However, we can Taylor expand Eqn. (25) around $\mathbf{I_{stim}^\top}$:

$$\begin{aligned}\bar{\nu}_\mathbf{t}^\top \approx& \phi(\mathbf{I_{stim}^\top}) + \phi'(\mathbf{I_{stim}^\top})\bar{\nu}_\mathbf{t}^\top \bar{\mathbf{w}}_\mathbf{t} \\ \Rightarrow \bar{\nu}_\mathbf{t}^\top \approx& \phi(\mathbf{I_{stim}^\top})[\mathbb{I} - \phi'(\mathbf{I_{stim}^\top})\bar{\mathbf{w}}_\mathbf{t}]^{-1},\end{aligned} \tag{26}$$

where $\mathbb{I}$ is the identity matrix. Moreover, if $\phi(\cdot)$ is a linear transformation such as $\phi(x) = \xi x$, the following relationship holds:

$$\begin{aligned} \bar{\nu}_{\mathbf{t}}^{\top} \approx & \xi(\mathbf{I}_{\mathbf{stim}}^{\top} + \bar{\nu}_{\mathbf{t}}^{\top} \bar{\mathbf{w}}_{\mathbf{t}}) \\ \Rightarrow \bar{\nu}_{\mathbf{t}}^{\top} \approx & \xi \mathbf{I}_{\mathbf{stim}}^{\top} [\mathbb{I} - \xi \bar{\mathbf{w}}_{\mathbf{t}}]^{-1}. \end{aligned} \tag{27}$$

Eqns. (26) and (27) shows that, if the weights are static ($\Delta \bar{\mathbf{w}}_{\mathbf{t}} = 0$), then the firing rate of the network converge towards an equilibrium. This observation is important because it highlights the fact that, in general, constant weights are needed to achieve a constant firing rate.

Eqn. (25) defines a relation determining plausible weight-frequency values, which in principle, are independent of the network's energy dynamics. In the Results section, we will explore how these constraints interact with the metabolic constraints at the network level.

Simulation's parameters

To numerically test our theoretical predictions, the network is simulated utilizing the Neural Simulation Tool program (NEST) [29] and the EDLIF neuronal model as well as the ED-STDP synaptic model are specified using NESTML [30], the domain-specific language tailored for the spiking neural network simulator NEST.

The simulated network has $n = 500$ neurons, and the excitatory-inhibitory ratio is $n_{ex} : n_{in} = 4 : 1$, following biologically realistic excitatory-inhibitory ratio values [31]. Fig. 4 shows the excitatory and inhibitory neurons randomly distributed in a $1\,mm^2$ surface area.

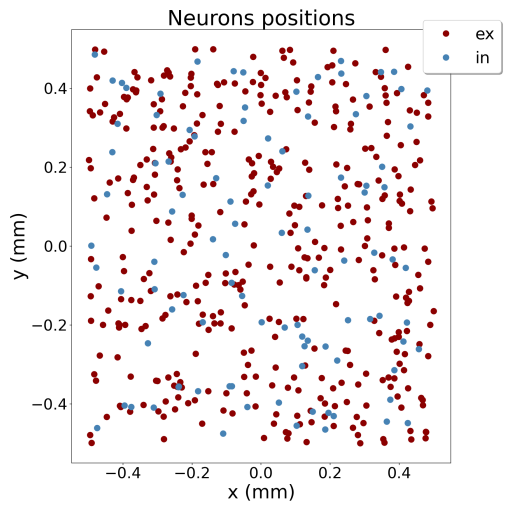

Fig 4. Excitatory-inhibitory balanced network.
Excitatory and inhibitory neuronal positions in a $1\,mm^2$ surface area. Each neuron x and y position is drawn from a random uniform distribution $U[-0.5, 0.5]$.

The network architecture is defined by an all-to-all connectivity. In addition, following *in vitro* measured weights strength in neuronal cell assemblies [32], initial synaptic strength values for the simulated network are drawn from an exponential distribution (see Eqn. (28))

$$f(w; \beta) = \begin{cases} \frac{1}{\beta} e^{-w/\beta}, & \text{if } w \geq 0, \\ 0, & \text{otherwise,} \end{cases} \tag{28}$$

Table 1. Parameters used when simulating the excitatory-inhibitory balanced network.

Parameter	Value	Unit
Δt_{sim}	0.1	ms
α	0.5	-
μ_-	0	-
μ_+	0	-
λ	0.01	-
τ_m	20	ms
τ_{ref}	8	ms
C_m	200	pF
v_{reset}	-70	mV
v_{rest}	-70	mV
v_{th}	-50	mV
τ_{syn}	6	ms
τ_{ap}	100	ms
I_{stim}	166 $\pm$ 15	pA
τ_{syn}^A	100	ms
E_{ap}	2	%
E_{syn}	0.5	%
E_{rp}	5	%
E_{hk}	5	%

where $f(w;\beta)$ is the probability density function of the exponential distribution. This means that the distribution of the weights w is described by an exponential distribution with scale parameter β. Therefore, the expected value of the weights is $\mathrm{E}[w] = \beta$ and the variance $\mathrm{Var}[w] = \beta$.

To emulate the incoming activity to each neuron from other brain areas, we inject into each neuron a constant current I_{stim} drawn from a Gaussian distribution with mean $\mu = 166\,pA$ and standard deviation $\sigma = 15\,pA$. By assuming that all neurons share the same parameters values we study the homogeneous parameter scenario (neuronal parameters are presented in Table 1),

Results

Energy-dependent plasticity and equilibrium

While studying static synapses and energy consumption in the neuron, closed-form expressions for available energy level in the cell were introduced. In Eqn. (16) the neuron's energy expenditure due to static synaptic activities is pondered by the normalized synaptic strength $\bar{w}_k$, however strength between neurons change over time (*i.e.,* $w_k := w_k(t)$). Here we analytically explore how the available energy in the neuron jointly with the synaptic sensitivity to energy imbalances η impact the synaptic plasticity between neurons. Specifically, we try to understand how metabolic constraints dictates synaptic plasticity equilibrium points, where synaptic potentiation and depression balance each other in average.

As we previously explained, our energy-dependent STDP rule uses postsynaptic available energy as a neuromodulator. Therefore, for low postsynaptic energy levels, potentiation is suppressed and the suppression depends on the sensitivity parameter η. For the following explanation let us assume equal synaptic time constants (*i.e.,* $\tau_+ = \tau_-$ in Eqn. (20)). Intuitively, given Eqn. (20) and $A(t = 0) = A_H$ initial postsynaptic

available energy, if peak potentiation is stronger than peak depression (*i.e.*, $\alpha \in [0, 1)$) then, for uniformly random pre- and postsynaptic spike times, in a short-time window simulation, weights tend to increase in average (see Fig. 5A).

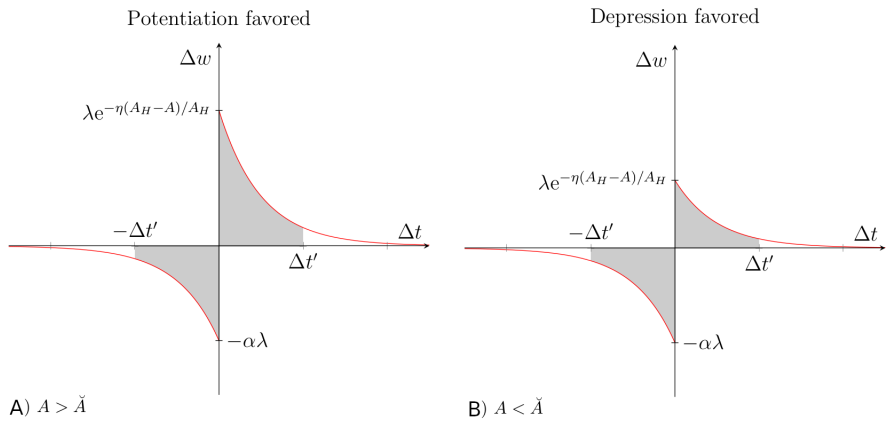

Fig 5. Energy-dependent plasticity and postsynaptic available energy. Potentiation suppression depends on postsynaptic energy level A. If $A > \breve{A}$ potentiation is favored (A), while for $A < \breve{A}$ depression is favored (B)

Higher weights induce more energy consumption in the postsynaptic neuron (because of the increased energy expenditure related to postsynaptic potentials and, also, because postsynaptic neurons will integrate more current, potentially increasing firing rate, which also contributes to energy consumption). Therefore, postsynaptic available energy decreases, suppressing potentiation. If potentiation is strongly suppressed then, for uniformly random pre- and postsynaptic spike times, in a short-time window simulation, depression will have a greater effect on weights, generating a net depression effect on weights (see Fig. 5B). This net depression force weights to decrease on average, thus decreasing the postsynaptic firing rate and also diminishing postsynaptic energy consumption. Consequently, postsynaptic available energy increases, favoring potentiation over depression, producing a potentiation depression loop (see Fig. 5). However, it is also possible that the postsynaptic available energy reaches an equilibrium level where potentiation and depression balance each other. Let us formally explain this intuition. If we assume random uniformly distributed inter-spike intervals $\Delta t = t_{post} - t_{pre}$:

$$\Delta t \sim U[-\Delta t', \Delta t']. \tag{29}$$

Given the postsynaptic available energy A, the net effect, also called drift, experienced by weights is the integral of Δw from Eqn. (20) over all possible Δt:

$$\int_{-\Delta t'}^{\Delta t'} \Delta w dt = \int_{-\Delta t'}^{0} -\lambda\alpha e^{t/\tau_-} dt + \int_{0}^{\Delta t'} \lambda e^{-\eta(A_H - A)/A_H} e^{-t/\tau_+} dt \tag{30}$$

$$= \lambda\Big[-\alpha\tau_- e^{t/\tau_-}\Big|_{-\Delta t'}^{0} - \tau_+ e^{\eta(A_H - A)/A_H} e^{-t/\tau_+}\Big|_{0}^{\Delta t'}\Big] \tag{31}$$

$$= \lambda[-\alpha\tau_-(1 - e^{-\Delta t'/\tau_-}) - \tau_+ e^{-\eta(A_H - A)/A_H}(1 - e^{-\Delta t'/\tau_+})] \tag{32}$$

If $\tau_+ = \tau_- = \tau_{syn}$, Eqn. (32) reads:

$$\int_{-\Delta t'}^{\Delta t'} \Delta w dt = \underbrace{\lambda\tau_{syn}(1 - e^{-\Delta t'/\tau_{syn}})}_{\geq 0}[-\alpha + e^{-\eta(A_H - A)/A_H}]. \tag{33}$$

Consequently, if $e^{-\eta(A_H-A)/A_H} > \alpha$, then potentiation is favored (*i.e.,* $\int_{-\Delta t'}^{\Delta t'} \Delta w dt \geq 0$). Whereas if $e^{-\eta(A_H-A)/A_H} < \alpha$ depression is favored. Similarly, by imposing $e^{-\eta(A_H-A)/A_H}{=}\alpha$ we can find the update weight fixed point (*i.e.,* $\Delta w = 0$), which gives the energy level $\breve{A}$ value for which potentiation and depression mutually balance each other:

$$\breve{A} = A_H\Big(1 + \frac{\ln(\alpha)}{\eta}\Big). \tag{34}$$

Eqn. (34) predicts the available energy level on the postsynaptic neuron for which, on average, potentiation and depression are compensated. Moreover, the equilibrium level for postsynaptic available energy $\breve{A}$ is inversely proportional to the sensitivity parameter η. As a consequence, if the plasticity rule is highly sensitive to energy imbalances, then Eqn. (34) guarantees that the postsynaptic energy level stay close to A_H (see Fig. 6).

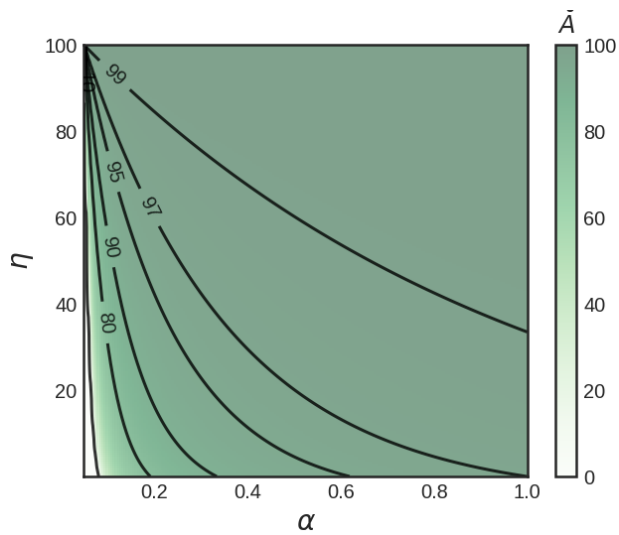

Fig 6. Available postsynaptic energy equilibrium level $\breve{A}$.
Postsynaptic energy equilibrium level $\breve{A}$ as a function of the sensitivity parameter η and depression scaling factor α. $A_H = 100\%$.

As we will explain, this fixed point is crucial for the network dynamics, because for $A = \breve{A}$ the weights are static (on average), thus average incoming current to the neuron should stay approximately constant if average is calculated over a time period T_w greater than membrane and synaptic time constant (*i.e.,* $T_w \gg \tau_m, \tau_{syn}$). Thus, we should expect a fixed point for the firing rate also.

Network's energy dynamic and fixed points under metabolic constraints

Built on the energy-dependent single-neuron model and the energy-dependent synaptic plasticity model, now we formalize, simulate, and investigate the dynamic and structure of E-I balanced networks including energy constraints in both, the single-neuron model as well as the synaptic plasticity. The developed models allow investigating how different sensitivities to energy imbalances at single neuron and synaptic level affect the network's dynamics and structure.

Energy dynamic and fixed point analysis

When studying the network's dynamics, we are particularly interested in knowing if the network converges or oscillates toward a specific state. If the network evolves toward an specific state independently of the initial conditions, those states are attractors of the network. Therefore, to find fixed points in the network dynamics, we start by trying to find if there are energy attractors in the network dynamics, when all the neurons share the same parameters (the homogeneous case). Accordingly, we analyze stable fixed points for energy states of an arbitrary neuron in the network.

Some caution should be taken before proceeding. When analyzing the fixed points of the network independently of the initial conditions, we mean that the network's state converges towards an attractor when considering a specific range of initial conditions. However, it is not completely independent of the initial conditions. For instance, if the inhibitory-excitatory weight values in the network are such that there is no excitatory activity (excitatory population has zero firing rate), then there are no weight updates in the networks and the network already is at a fixed point. Therefore, in what follows, we are assuming that the initial conditions allow significant excitatory and inhibitory activity, thus avoiding the study of *trivial solutions* as the one previously explained.

The total energy change $\Delta A(t) = A(t+T) - A(t)$ of any neuron in the network in a time interval T is calculated by summing the contributions of energy production and consumption occurring in the time interval $[t, t+T]$. From Eqn. (6) we obtain:

$$\Delta A(t) = \int_t^{t+T} A_s(t') - A_c(t')dt'. \tag{35}$$

Previously, we formalized the synaptic energy consumption A_{syn} (see Eqn. (11)) as well as the neuron's own action potential energy consumption A_{ap} (see Eqn. (13)), for arbitrary ε_{syn} and ε_{ap} kernels. To simplify the mathematical tractability, now we will choose the delta kernel $\varepsilon(t-t_s) = \delta(t-t_s)$ for ε_{syn} and ε_{ap}. Thus, Eqn. (35) reads:

$$\frac{1}{T}\Delta A(t) = \frac{1}{T}\int_t^{t+T} K(A_H - A(t'))dt' - E_{ap}\frac{1}{T}\int_t^{t+T}\sum_{spike\ s}\delta(t'-t_s)dt' - \tag{36}$$

$$E_{syn}\frac{1}{T}\int_t^{t+T}\sum_{synapse\ k}\sum_{spike\ s}\bar{w}^k(t')\delta(t'-t_s)dt'. \tag{37}$$

Because weights change slowly (*i.e.,* $\lambda \ll 1$ in Eqn. (20)), for small T we can assume they are constant in the $[t, t+T]$ interval (*i.e.,* $\bar{w}^k(t) = \bar{w}^k_t$). Formally, we are assuming that time scales of learning and neuronal spike dynamics can be separated [33]. In addition, because of the linearity of the integral operator:

$$\begin{aligned}\frac{1}{T}\Delta A(t) =& K(A_H - \bar{A}_t) - E_{ap}\frac{1}{T}\sum_{spike\ s}\delta(t-t_s) - E_{syn}\frac{1}{T}\sum_{synapse\ k}\sum_{spike\ s}\bar{w}^k_t\delta(t-t_s)\\ =& K(A_H - \bar{A}_t) - E_{ap}\bar{\nu}_t - E_{syn}\sum_{synapse\ k}\bar{w}^k_t\bar{\nu}^k_t,\end{aligned} \tag{38}$$

where $\bar{A}_t = T^{-1}\int_t^{t+T} A(t')dt'$ is the mean energy level of the neuron in the $[t, t+T]$ interval, and in the second and third terms we obtain the neuron self and connected neighbor's firing rates, respectively ($T^{-1}\int_t^{t+T}\sum_{spikes\ s}\delta(t'-t_s)dt'$). Now, if we impose ΔA=0 in Eqn. (38), it is possible to find neuron's firing rates, incoming weight, and energy expenditure values that satisfy the energy fixed point constraints:

$$\bar{A}_t = A_H - \frac{1}{K}\Big[E_{ap}\bar{\nu}_t + E_{syn}\sum_{synapse\ k}\bar{w}^k_t\bar{\nu}^k_t\Big], \tag{39}$$

which in matrix form reads:

$$\bar{\mathbf{A}}_{\mathbf{t}}^{\top} = \mathbf{A_H}^{\top} - \frac{1}{K}\bar{\nu}_{\mathbf{t}}^{\top}\Big[E_{ap}\mathbb{I} + E_{syn}\bar{\mathbf{w}}_{\mathbf{t}}\Big], \tag{40}$$

where $\bar{\mathbf{A}}_{\mathbf{t}} = [\bar{\mathbf{A}}_{\mathbf{t}}^{\mathbf{ex}\top}, \bar{\mathbf{A}}_{\mathbf{t}}^{\mathbf{in}\top}]^{\top}$. Eqn. (39) holds if the neuron is in an energy fixed point and, to achieve the energy fixed point, the excitatory-excitatory connections to the neuron under study also need to achieve a fixed point (the other connections are static). Otherwise, the synaptic energy consumption (A_{syn}) will stay varying, impeding to achieve an energy fixed point in the postsynaptic excitatory neuron. Please realize that, if the excitatory-excitatory connections achieve a fixed point as well as the presynaptic neuron's firing rate, then the firing rate of the postsynaptic neuron also achieves a fixed point (*i.e.,* $\Delta\bar{\nu}_t = 0$).

Excitatory-excitatory connections stabilize at a fixed point when the postsynaptic excitatory neuron's energy level matches $\breve{A}$. We're setting aside the so-called *trivial solutions* where the neuron's firing rate, represented as $\bar{\nu}_t$, is zero. With $\bar{\nu}_t = 0$ (and consequently $\Delta\bar{\nu}_t = 0$), there aren't any spikes to modify the neuron's incoming weights. As a result, these incoming weights remain unchanged, leading to a constant energy level in the neuron ($\Delta A = 0$), regardless of whether $\bar{A}_t \not\approx \breve{A}$. Therefore, silence neurons (neurons with firing rate $\bar{\nu}_t$ equal to zero) conform to Eqn. (39). If there's no rise in their incoming current, they will stay at the fixed point where $\Delta A = \Delta w = \Delta\nu = 0$, even without needing to meet the $\bar{A}_t \approx \breve{A}$ condition. Thus, for non-silent neurons in the fixed point, we can approximate $\bar{A}_t \approx \breve{A}$, obtaining:

$$\begin{aligned}\breve{A} \approx & A_H - \frac{1}{K}\Big[E_{ap}\bar{\nu}_t + E_{syn}\sum_{synapse\ k}\bar{w}_t^k\bar{\nu}_t^k\Big] \\ A_H\Big(1 + \frac{\ln(\alpha)}{\eta}\Big) \approx & A_H - \frac{1}{K}\Big[E_{ap}\bar{\nu}_t + E_{syn}\sum_{synapse\ k}\bar{w}_t^k\bar{\nu}_t^k\Big].\end{aligned} \tag{41}$$

By rearranging (41), we arrive to the following relationship constraining weights and firing rates of each neuron in the network:

$$-\frac{A_H K\ln(\alpha)}{\eta} \approx E_{ap}\bar{\nu}_t + E_{syn}\sum_{synapse\ k}\bar{w}_t^k\bar{\nu}_t^k. \tag{42}$$

If all the neurons in the network converge towards a fixed point, they must satisfy Eqn. (39) and, in particular, non-silent excitatory neurons must satisfy Eqn. (42). In consequence, in this state, all the excitatory-excitatory connections in the network remain constant (*i.e.,* $\Delta\bar{w}_t = 0$) in average as well as the firing rates (*i.e.,* $\Delta\bar{\nu}_t = 0$). As a result, Eqn. (42) allow us to predict the energy consumption of each non-silent excitatory neuron in the network after converging towards a fixed point.

However, under certain conditions, such as the neuron under study has $n \gg 1$ synapses, high E_{syn} values or strong incoming w weights, it is possible to neglect the neuron's own action potentials energy consumption (*i.e.,* $E_{ap}\bar{\nu}_t \ll E_{syn}\sum_k \bar{w}_t^k\bar{\nu}_t^k$), thus we approximate (42) by:

$$\begin{aligned}-\frac{A_H K\ln(\alpha)}{\eta E_{syn}} &\approx \sum_{synapse\ k}\bar{w}_t^k\bar{\nu}_t^k \\ &= \sum_{ex\to ex\ synapse\ k}\bar{w}_t^{ex\to ex,\ k}\bar{\nu}_t^{ex,\ k} + \sum_{in\to ex\ synapse\ k}\bar{w}_t^{in\to ex,\ k}\bar{\nu}_t^{in,\ k}.\end{aligned} \tag{43}$$

Consequently,

$$\underbrace{-\frac{A_H K \ln(\alpha)}{\eta E_{syn}} - \sum_{in\to ex\ synapse\ k} \bar{w}_t^{in\to ex,\ k} \bar{\nu}_t^{in,\ k}}_{\Lambda} \approx \sum_{ex\to ex\ synapse\ k} \bar{w}_t^{ex\to ex,\ k} \bar{\nu}_t^{ex,\ k}. \quad (44)$$

Eqn. (39) reveals a metabolic constraint over incoming synapse strengths and their respective presynaptic neuronal firing rates, affecting non-silent excitatory neurons in the energy fixed point. In particular, Eqn. (42) shows that, to achieve a metabolic fixed point in the excitatory postsynaptic neurons, there is a trade-off between synaptic strength and the corresponding presynaptic neuronal firing rate. Interestingly, the metabolic constraint in Eqn. (42) dictates an inverse relationship between weights and firing rates, which is a completely new constraint in the system, given that previous models generally do not account for metabolic activity. Moreover, the constraint mentioned above enables the emergence of an attractor state to the network, as a consequence of the interception between the metabolic and the physically plausible states of the network given by the previously introduced metabolic (see Eqn. (42)) and weight-frequency relations (see Eqn. (25)).

On the one hand, Eqn. (25) gives a weight-rate relationship where increasing excitatory-excitatory weights $\mathbf{w^{ex\to ex}}$ generates higher excitatory firing rates $\nu^{\mathbf{ex}}$, due to higher mean incoming synaptic currents to postsynaptic neurons. On the other hand, if either excitatory-excitatory weights or excitatory firing rates increase, the postsynaptic energy levels drop (see Eqn. (40)). In addition, at the metabolic fixed point and under previously described assumptions, non-silent excitatory neurons fulfill Eqn. (44). As a consequence, if excitatory firing rates (excitatory-excitatory weight) increase, then excitatory-excitatory weights (excitatory firing rates) must decrease. Thus, Eqn. (44) imposes an inverse relationship between excitatory-excitatory weights and excitatory firing rates, contrary to Eqn. (25), where the relationship between the two variables is direct. Fig. 7 shows a conceptualization of the previous reasoning.

With an analytical understanding of how metabolic constraints affect the structure and dynamics of the network, let us now explore the impact of metabolic constraints on the network through numerical simulations.

Network activity and structure without energy constraints

Before analyzing the network's structure and dynamics under energy constraints on simulations, we first simulate the network without energy constraints (*i.e.,* $\gamma = \eta = 0$). Thus, the current-rate relation from Eqn. (25) as well as the available energy in the neuron dictated by Eqn. (40) holds, but Eqn. (42) does not hold, because Eqn. (42) holds for the excitatory population only if energy constraints are affecting $\mathbf{w^{ex\to ex}}$ plasticity (*i.e.,* $\eta > 0$).

Simulating the network without metabolic constraints is useful as a base case for comparisons before including metabolic constraints (all the simulations presented in the Results section have the same initial conditions). Fig. 8 shows the network's dynamics and structure when no metabolic constraints are included. As expected, firing rates increase until saturation due to favored synaptic potentiation ($\alpha = 0.5$). In this regard, the refractory period for each neuron in the network is $\tau_{ref} = 8\,ms$. Thus, the maximum theoretical firing rate for an infinite stimulation current is $\tau_{ref}^{-1}\,kHz \Rightarrow \nu_{max} = 125Hz$ (see Eqn. (21)). Therefore, the network's firing rate is close to the saturation state. Moreover, the mean energy level of the excitatory population (Fig. 8) decreases until stabilizing at $A(t) \approx 75\%$. The energy stabilization point occurs at the firing rate and excitatory-excitatory strength saturation. The previous

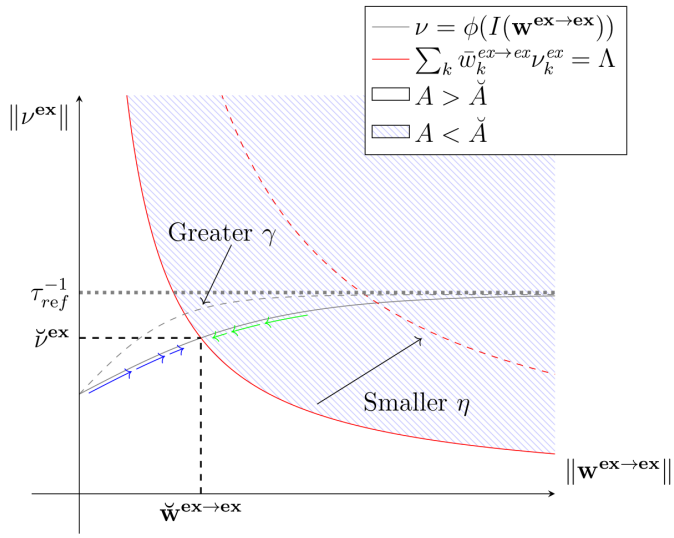

Fig 7. Energy-dependent E-I balanced network and constraints intersection. The gray curve describes excitatory firing rate magnitude as a function of excitatory-excitatory weights magnitude (see Eqn. (25)), whereas the red curve conceptualizes the inverse relation between excitatory firing rates and excitatory-excitatory weights magnitudes given by metabolic constraints (see Eqn. (44)) affecting non-silent excitatory neurons in the energy fixed-point. On the blue region, the postsynaptic energy level drops below the energy level fixed-point $\breve{A}$. Thus, in the blue region, $\mathbf{w}^{\mathbf{ex}\to\mathbf{ex}}$ experience a net depression drift (see Eqn. (32)), whereas in the white region, the postsynaptic energy level is above $\breve{A}$. Consequently, in the white region, there is a net potentiation drift. Therefore, if the network state is in the blue region, energy-dependent plasticity rules push the network state toward the intersection between the two curves (following the green arrows). Likewise, if the network is in the white region, energy-dependent plasticity pushes the network state toward the intersection point between the two curves (following the blue arrows). Finally, in the intersection between the two curves (the system's metabolic fixed point) the postsynaptic energy level is $\breve{A}$ and, as a consequence, $\Delta\mathbf{w}^{\mathbf{ex}\to\mathbf{ex}} = 0$ on average.

observation is supported by realizing that if firing rates and excitatory-excitatory weights are saturated, the energy consumption in each neuron can be approximated by:

$$\begin{aligned} A_c \approx & E_{syn} \sum_k \bar{w}_k \bar{\nu}_k \\ \approx & E_{syn} \times n_{ex} \times \bar{w}_{max} \times \nu_{max} \\ = & 0.5 \times 400 \times 1 \times 0.125 \\ = & 25\%, \end{aligned}$$

in agreement with what is observed in Fig. 8 However, in principle, without energy constraints, each neuron's energy level can decrease until achieving $A(t) = 0$. This is the case if we, for instance, sufficiently increase the number of neurons in the network, or increase the energy consumption related to postsynaptic potentials E_{syn}. Eqn. (39) describes which variables affect energy consumption and the available energy in the neuron.

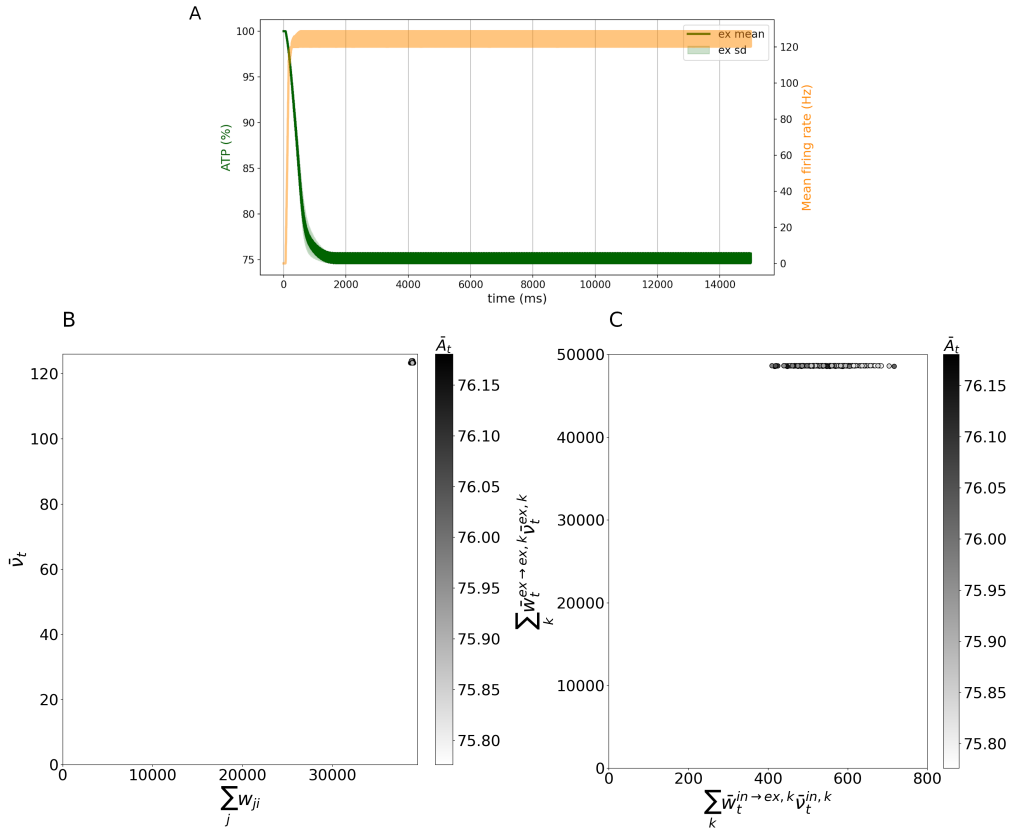

Fig 8. Network dynamic and structure without energy constraints. Network simulation when there are no metabolic constraints in the network. Mean available energy in the excitatory population keeps dropping until neuronal firing rates are saturated. Figure (A) shows mean energy level and mean firing rate for the excitatory population, while Figure (B) shows final incoming synaptic strength per neuron ($\sum_j w_{j,i}$) and mean firing rate per neuron. The mean firing rates in Figures (B) and (C) are calculated considering the last 10% of the simulation.

Exploring synaptic energy imbalances sensitivity η

From our previous theoretical developments, for higher synaptic energy imbalance sensitivities η we expect higher energy level equilibrium values $\breve{A}$ (Eqn. (34)). To achieve $\breve{A}$ closer to A_H, energy consumption needs to decrease, and postsynaptic energy consumption decreases if the presynaptic rate decreases, or if incoming synaptic strengths decrease (Eqn. (43)). Therefore, as we increase η, lower firing rates as well as weaker excitatory-excitatory synaptic strengths are expected as Fig. 7 conceptually represents. In addition, to satisfy Eqn. (43) an inverse relation between $\sum_k \bar{w}_t^{in\to ex,\ k}\bar{\nu}_t^{in,\ k}$ and $\sum_k \bar{w}_t^{ex\to ex,\ k}\bar{\nu}_t^{ex,\ k}$ should be observable in the simulations.

Fig. 9 shows the mean available energy and neuronal firing rate through the simulation, for the excitatory population. Consistently with Eqn. (34), while synaptic energy imbalance sensitivity η increases, the energy level equilibrium point increases and stays close to our analytical prediction (dashed gray line). Also, while the energy fixed-point $\breve{A}$ increases, the mean neuronal firing rate decreases, which aligns with the theoretical description represented in Fig. 7.

The first column of Fig. 10 shows neuronal firing rate as a function of incoming synaptic strength, for different synaptic sensitivities η values. In agreement with Eqn. (25), as the incoming synaptic strengths increases, the firing rate increases. Also, when η increases, neuronal rates and excitatory-excitatory weights decrease, as it can be observed from Fig. 10A with $\eta = 30$ having higher firing rates and stronger excitatory-excitatory synapses than the ones observed in Fig. 10C where $\eta = 50$. The previous observation is also valid when contrasting Fig. 10C where $\eta = 50$ against Fig. 10E where $\eta = 100$; when synaptic sensitivity η increases, excitatory firing rates tend to decrease.

Regarding the inverse relation between $\sum_k \bar{w}_t^{in\to ex,\ k}\bar{\nu}_t^{in,\ k}$ and $\sum_k \bar{w}_t^{ex\to ex,\ k}\bar{\nu}_t^{ex,\ k}$ dictated by Eqn. (43), the second column of Fig. 10 shows the relationship between these two variables for simulations with increasing η. For a low synaptic sensitivity to energy imbalance, there seems to be an inverse relation in Fig. 10B, although not very clear. However, if synaptic sensitivity η increases, the inverse relationship between the two variables becomes more evident, as shown in Fig. 10D. Interestingly, when the synapses are highly sensitive to energy imbalance (Fig. 10E and 10F), it is not possible for all the neurons to achieve the metabolic fixed point, and some neurons achieve the silent fixed point previously described.

When there is an extreme synaptic sensitivity to energy imbalances (Fig. 10E) and 10F), a subpopulation of excitatory neurons remains silent (neurons with zero firing rate in Fig. 10E). It is not surprising that silent neurons have higher inhibitory weights (black dots in Fig. 10F). This happens because just before the separation of the network into two subpopulations ($t \approx 7000ms$), there is a slight decrease in available energy coexisting with an increase in firing rate, followed by an increase in available energy join with a reduction in firing rate. This last increment in available energy must be accompanied by a general decrease in excitatory-excitatory weights ($A < \breve{A}$ implies a net negative drift in excitatory-excitatory weights). If there is a general decrement in excitatory-excitatory weights, then the first neurons to be silent are the ones with higher inhibitory incoming weights. After entering the silent state, their excitatory-excitatory weights remain constant, so the only possibility for them to stop being silent, is to receive higher incoming current, but this is not possible, because the silent neurons allow decreasing the energy consumption in the non-silent neurons such as the non-silent neurons can satisfy the metabolic fixed-point where $A \approx \breve{A}$. As a consequence, the silence of those neurons enables the network to converge toward a stable fixed point, with one subpopulation staying in the metabolic fixed point, while another subpopulation stays in the silent fixed point. In this scenario, one group of neurons still tries to satisfy the $\bar{A}_t \approx \breve{A}$ energy constraints, and their energy equilibrium point is

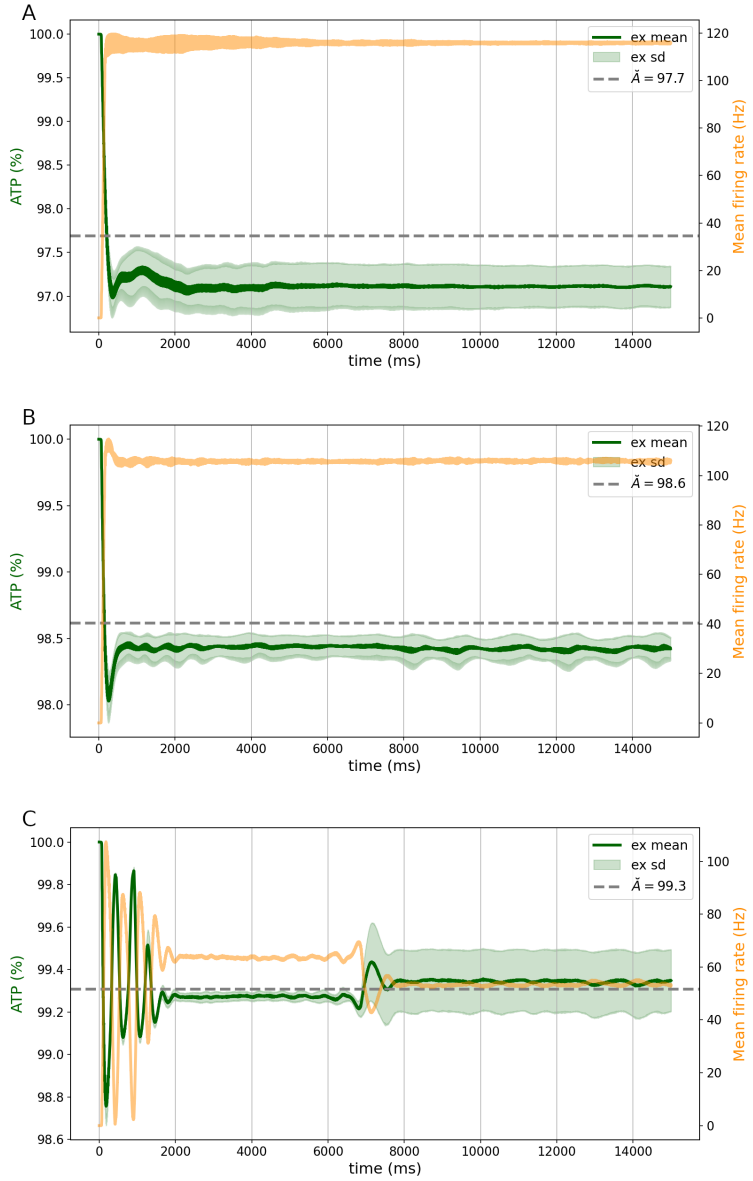

Fig 9. Mean available energy and firing rate for different synaptic sensitivities to energy imbalances.
A is obtained with $\eta = 30$ parameter, while for B $\eta = 50$, and $\eta = 100$ in C. Figures show the mean energy level and firing rate for the excitatory population, and there is no neuronal sensitivity to energy imbalances (*i.e.*, $\gamma = 0$).

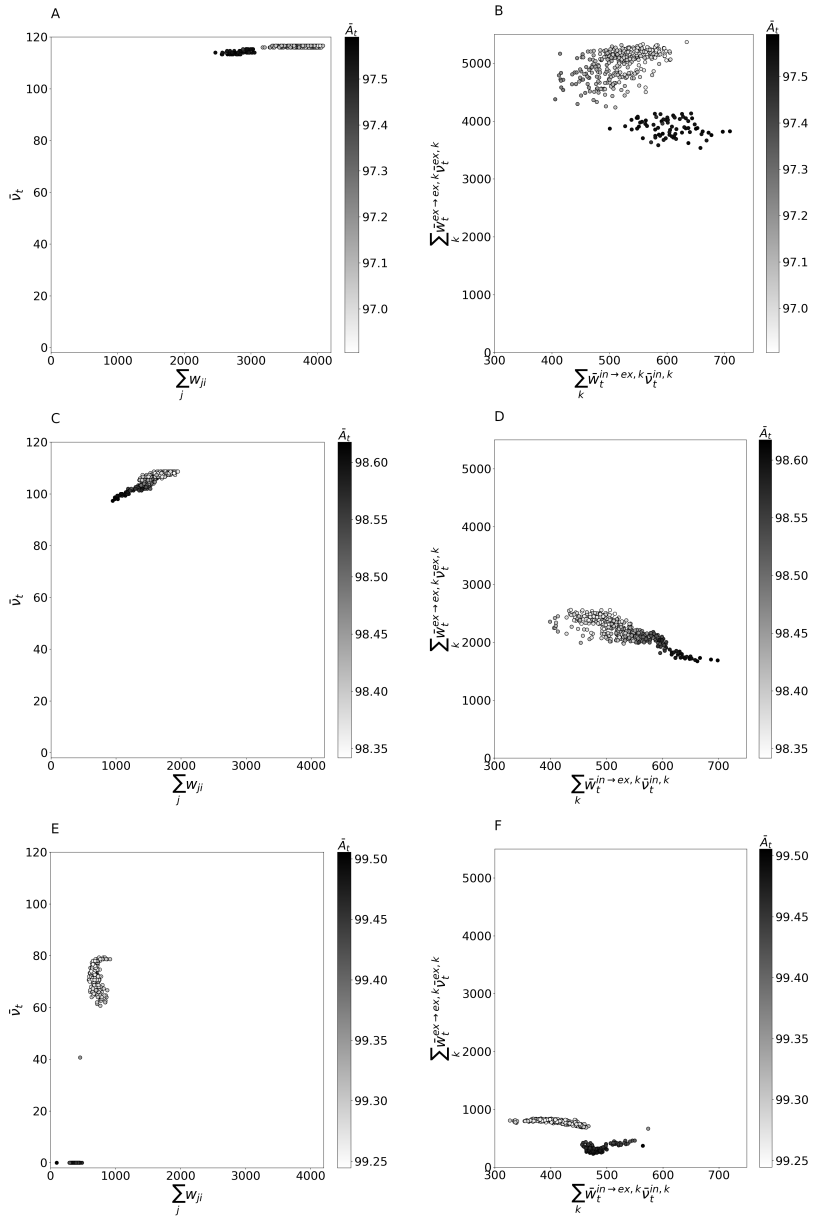

Fig 10. Weight-rate and synaptic energy consumptions when the synaptic sensitivity to energy imbalances varies.
The Figures in the first column show the mean firing rates versus incoming synaptic strengths, thus the numerically equivalent to the current-rate mapping defined by $\phi(\cdot)$. The Figures in the second column show the energy consumption in each neuron due to presynaptic excitatory neurons and presynaptic inhibitory neurons. Figures (A) and (B) are obtained with $\eta = 30, \gamma = 0$ parameter values, while for Figures (C) and (D) $\eta = 50, \gamma = 0$. finally, figures (E) and (F) show the simulations results when $\eta = 100, \gamma = 0$. The mean firing rates $\bar{\nu}_t$ in all cases were calculated considering the last 10% of the simulation.

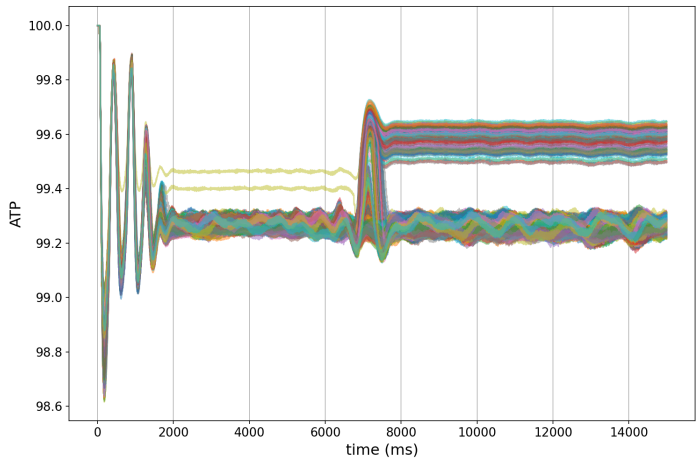

Fig 11. Excitatory population separations.
The excitatory population divides into two subpopulations due to high synaptic sensitivity to energy imbalances η. The silent subpopulation has higher available energy ($ATP \sim 99.6\%$).

close to the one predicted by Eqn. (42), as shown in Fig. 11. The second group of silent neurons has a higher available energy, but their energy consumption is different than zero. This is not the only case in which there must be silent neurons to achieve a global fixed point. For instance, if the neuronal population is huge, then this phenomenon also occurs (although there is no need for extreme synaptic sensitivity to energy imbalances in this case), or if a metabolic impairment is simulated, as we will show later. The separation of excitatory populations in two subpopulations can be interpreted as a specialization. Surprisingly, under the developed framework, silent neurons emerge as a consequence of local energy constraints in the network and, if this silent neurons are not present, then it is not possible to achieve a global fixed point in the network.

Including neuronal sensitivities to energy imbalances γ

So far, the developed theoretical analysis of the energy-dependent network does not account explicitly for neuronal energy imbalance sensitivity γ. However, we know that neuronal sensitivity to energy imbalances γ affects neuronal firing rate. Thus, we can include the neuronal sensitivity parameter in the current-rate mapping $\phi(\cdot) := \phi_\gamma(\cdot)$. In particular, if the energy level in a neuron is below the homeostatic energy level (*i.e.,* $A \leq A_H$), for the same incoming input current, the neuron's firing rate is higher for higher γ, as demonstrated by Eqn. (5) and shown in Fig. 1. Consequently, if two networks (A and B) are equal (in particular, have the same initial excitatory-excitatory weights), but the neurons in network A have higher γ sensitivity than neurons in network B, then network A must have higher or equal excitatory firing rates than network B. As a consequence, to achieve an energy equilibrium point, network A needs to decrease excitatory-excitatory synaptic strengths. This idea is conceptualized in Fig. 7 with the gray dashed line representing the current-rate mapping when γ is increased. Following the previous explanation, for higher γ we expect the network to have weaker excitatory-excitatory synaptic strengths as well as higher firing rates.

To numerically explore the effect of modifying γ, we maintain synaptic sensitivity

$\eta = 50$ fixed and vary the neuronal sensitivity to energy imbalances γ. Because the synaptic sensitivity η is constant for all cases in Fig. 12 and the energy level fixed point is independent of the neuronal sensitivity parameter γ, the theory predicts that networks with different neuronal sensitivity γ (and all other parameters being equal) should converge towards the same energy level. The previous prediction is confirmed by observing Fig. 12, where for different γ values, the energy fixed points are almost the same. However, as already anticipated by the theory, in the metabolic fixed point, higher γ value are associated with higher mean excitatory firing rates $\bar{\nu}_t^{ex}$. This prediction is confirmed by calculating the mean excitatory firing rate $\bar{\nu}_t^{ex}$ considering the last 10% of the simulation for each case. Particularly, when $\gamma = 10$ we obtain $\bar{\nu}_t^{ex} = 106.5$, while for $\gamma = 20$ the mean excitatory firing rate ($\bar{\nu}_t^{ex}$) is 107.6, finally for $\gamma = 50$ we obtain $\bar{\nu}_t^{ex} = 111.1$. Although not easily recognizable, this pattern is also observable by comparing the weight-rate relationship in Fig. 13 for each case. When $\gamma = 10$ (Fig. 12A) the firing rate is slightly lower compared with the $\gamma = 20$ case (Fig. 12B). Moreover, this relation also holds when comparing the $\gamma = 20$ case against the $\gamma = 50$ case (Fig. 12C). The first column in Fig. 13 shows the experimental current-rate relationship for excitatory neurons in the network. In agreement with the previous explanation and with Fig. 7, as neuronal sensitivity γ increases from Fig. 13A to 13B and 13C, numerical experiments show that neurons become more easily excitable. Thus, generating higher firing rates when γ is higher. Further, if we observe the second column in Fig. 13, it is clear that the relationship defined by Eqn. (43) is satisfied, thus respecting the relationship between $\sum_k \bar{w}_t^{in\to ex,\ k}\bar{\nu}_t^{in,\ k}$ and $\sum_k \bar{w}_t^{ex\to ex,\ k}\bar{\nu}_t^{ex,\ k}$.

Regarding excitatory-excitatory synaptic strength, simulations shows that excitatory-excitatory weight slightly decreases as neuronal sensitivity γ increases This observation is supported by realizing that when γ increases, the energy fixed point does not change, but the firing rates increases (Fig. 12).This is only possible because the excitatory-excitatory weights decrease, compensating the increased firing rates and thus allowing to keep the same energy consumption. Thus, the theoretical predictions regarding the effect of increasing γ while keeping η fixed is proved and in well agreement with numerical experiments.

Impaired metabolic production

Regarding biology, our theoretical and simulation framework allows us to study what happens when impaired metabolic production affects neurons. This question is relevant because evidence suggests that metabolic impairments are a common cause for various neurodegenerative diseases [4–9]. Therefore, improving the understanding of how metabolic impairments affect network dynamics and structure is potentially valuable fro clinical purposes.

From our theoretical developments, if the ATP rate production controlled by parameter K decreases, we expect:

1. Given that the energy level equilibrium point for non-silent neurons $\breve{A}$ guaranteeing $\Delta w^{ex\to ex} = 0$ on average is independent of K (see Eqn. (34)), if there is a mean energy level fixed point for non-silent neurons, it should stay constant as K varies.

2. By analyzing Eqn. (43), for non-silent neurons, if K decrease, $\sum_k \bar{w}_t^{in\to ex,\ k}\bar{\nu}_t^{in,\ k}$ or $\sum_k \bar{w}_t^{ex\to ex,\ k}\bar{\nu}_t^{ex,\ k}$ needs to decrease in order to satisfy the aforementioned metabolic relation. The only plastic synapses in the network are $\mathbf{w^{ex\to ex}}$. Therefore, if the metabolic production is impaired, we expect lower firing rates as well as weaker excitatory-excitatory synaptic strengths.

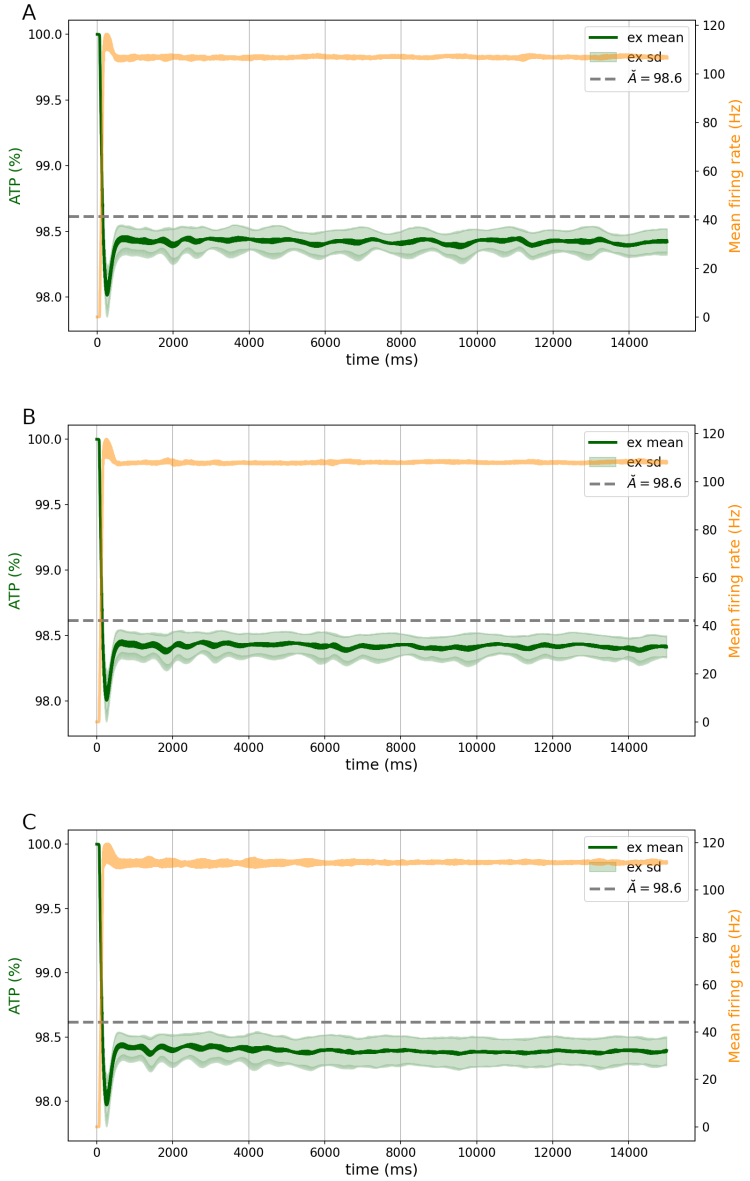

Fig 12. Mean available energy and firing rate for different neuronal sensitivities to energy imbalances.
(A) is obtained with $\eta = 50, \gamma = 10$ parameter values, while for (B) $\eta = 50, \gamma = 20$, and $\eta = 50, \gamma = 50$ in (C). Figures show the mean energy level and firing rate for the excitatory population.

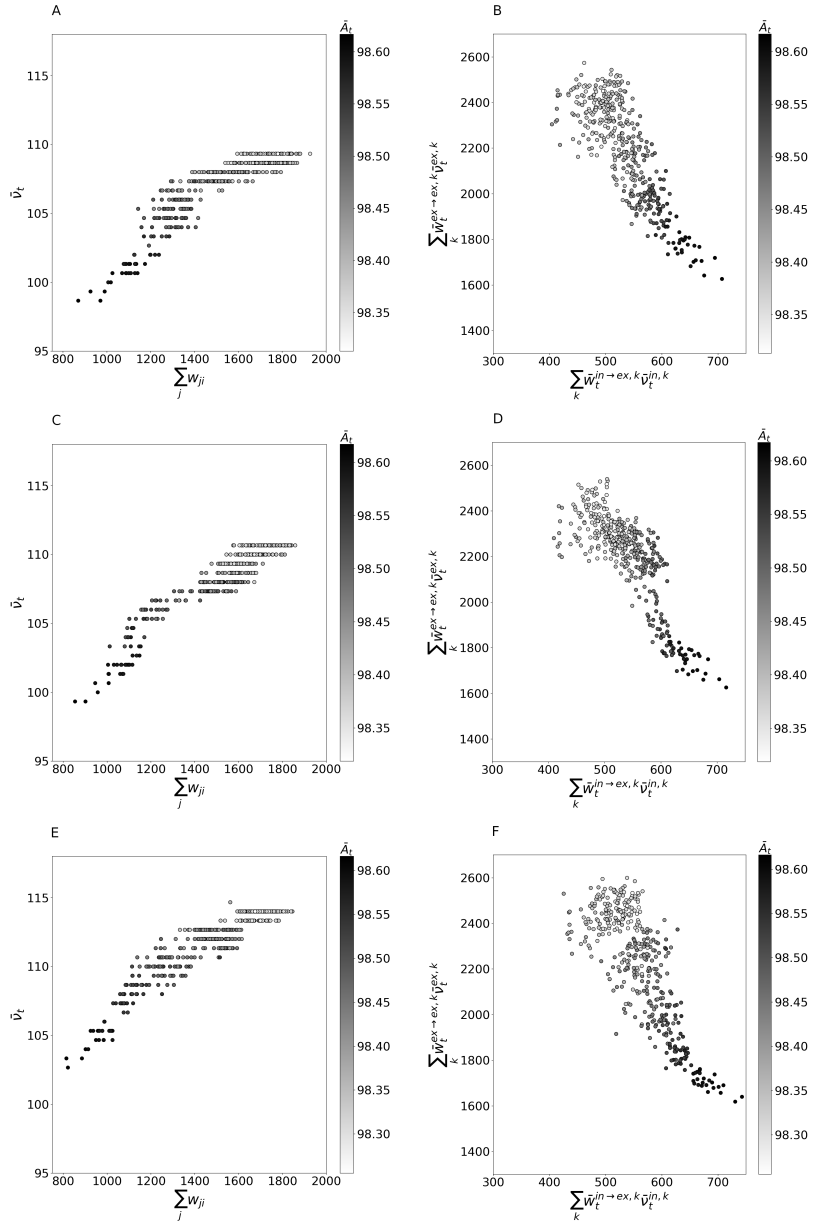

Fig 13. Weight-rate and energy consumptions when neuronal sensitivity to energy imbalances varies.
The Figures in the first column show mean firing rates versus incoming synaptic strengths, thus the numerically equivalent to the current-rate mapping defined by $\phi(\cdot)$. The Figures in the second column show the energy consumption in each neuron due to presynaptic excitatory neurons and presynaptic inhibitory neurons. Figures (A) and (B) are obtained with $\eta = 50, \gamma = 10$ parameter values, while for Figures (C) and (D) $\eta = 50, \gamma = 20$. Finally, Figures (E) and (F) show the simulation results when $\eta = 50, \gamma = 50$. The mean firing rates $\bar{\nu}_t$ in all cases were calculated considering the last 10% of the simulation.

3. By analyzing Eqn. (9) and the fact that the time constant of the energy production in the neuron is $\tau_A = 1/K$, we know that lower production rate K values are associated with slower production responses. As a consequence, if a neuron with impaired metabolic production is subjected to an abrupt constant energy consumption, the energy production response to that consumption will be slower than the energy production response of a *healthy* neuron. In addition, this abrupt energy consumption will pull the neuron's available energy to a lower level compared to a *healthy* neuron subjected to the same energy consumption. Formally, we can describe an abrupt and constant consumption as a step energy consumption $A_c(t) = \Theta(t')A_c$ starting at time $t = t'$. Given enough time, the available energy of a neuron subjected to such energy consumption is $A = A_H - \frac{A_c}{K}$. Given the slower response to energy consumption in the impaired case, producing higher delays between energy production and consumption, we expect to observe more oscillations in the ATP dynamics when simulating the network.

For the metabolically impaired simulations we vary K, but keep the synaptic sensitivity to energy imbalances $\eta = 50$ and the neuronal sensitivity $\gamma = 20$ (Figs 12B, 13C and 13D shows the *healthy* base case for comparison, where there is no metabolic impairment in energy production).

Fig. 14 shows the mean available energy level and firing rate of the network through the simulations. In particular, Fig. 14A is obtained when $K = 0.7$. Please note that the numerical energy level fixed point when $K = 0.7$ is very close to the one obtained with $K = 1$ simulation (Fig. 12B), confirming that if there is an energy fixed point for non-silent neurons, it is independent of the ATP rate production K, in agreement with our first theoretical prediction. Moreover, if we compare Figs 13D and 15B, it is clear that both simulations satisfy the energy relationship defined by Eqn. (43). However, in Fig. 13D ($K = 1$) the mean $\sum_k \bar{w}_t^{ex\to ex,\ k} \bar{\nu}_t^{ex,\ k}$ energy consumption is much higher than the one consumed in Fig. 15B when $K = 0.7$, in agreement with the second theory prediction. Besides, contrasting Fig. 12B and 14B, a decrease in mean firing rate (orange curve) for the excitatory populations is observed when ATP rate production K decreases, also in agreement with the second prediction from theory. The decrease in excitatory population firing rate when K decreases can also be observed by contrasting Fig. 13C ($K = 1$) and Fig. 15A ($K = 0.7$). Therefore, if energy production is impaired in any neuron, then the energy consumption of that neuron needs to decrease to achieve a fixed point.

Hence, if we keep decreasing K (higher production impairment), energy consumption needs to drop to be consistent with the theory. In Figs 14B, 15C and 15D the ATP rate production is $K = 0.5$. Although the mean average rate and excitatory-excitatory weights decrease (Figs 14B and 15D, respectively) concerning the $K = 0.7$ case, when $K = 0.5$ the convergence towards a global fixed point is possible when a subpopulation of the network becomes silent. This behavior agrees with the energy constraints imposed on the network. In particular, as previously explained, if the ATP rate production parameter K decreases, then the energy consumption needs to drop. To decrease energy consumption, excitatory-excitatory weights decrease and, consequently, mean excitatory firing rates decrease. Then, silencing a subpopulation of neurons is a consequence of a strict policy toward diminishing energy consumption. Even though this is a similar phenomenon to the one observed when there is a high synaptic sensitivity to energy imbalances (Figs 9C, 10F, 10E and 11), it is not the same, because the cause of the phenomenon is different. When there is a high synaptic energy imbalance sensitivity η, the energy level fixed point is close to the homeostatic energy level A_H (Eqn. (34)), thus decreasing energy consumption is necessary to converge towards a global fixed point. In contrast, in the metabolic production impairment case, the energy level fixed point is

not necessarily close to the homeostatic energy level A_H. However, because energy production is impaired, energy consumption needs to drop to achieve an energy fixed point. Therefore, in the high synaptic energy imbalance sensitivity case, the energy consumption drops because the energy level fixed point needs to be close to A_H in order to achieve $\Delta w \approx 0$, which is a constraint imposed by the synapses. While in the metabolically impaired case, the energy consumption needs to drop because neuronal on-demand energy production cannot compensate for high energy consumption, and this compensation between energy consumption and production is a requirement for the network to reach a fixed point. Therefore this is a constraint imposed by neurons, not by the synaptic energy sensitivity, thus decreasing energy consumption is necessary to achieve the energy fixed point. However, despite both phenomena being different, in the metabolic impaired case again the silent neurons are the ones with higher inhibitory synapses, and the reason is the same as in the case where high synaptic sensitivity to energy imbalances is present: before the network separates into two subpopulations there is an increase in available energy accompanied by a global excitatory-excitatory weights strength's decrease. If all the excitatory neurons receive a decreasing incoming current, the first in becoming silent are the ones that have higher inhibitory weights.

If we continue aggravating the metabolic production impairment and the network is able to achieve a fixed point, theoretically, we expect even weaker excitatory-excitatory synaptic strengths as well as lower firing rates in the equilibrium state. Accordingly, we simulate the network with $K = 0.1$, emulating the case where neurons can produce energy at a 10% rate with respect to the healthy case (*i.e.,* $K = 1$). Fig. 14C shows that the energy production is so impaired that the network is not able to achieve an equilibrium point and stays oscillating, exploring excitatory-excitatory weights strengths which allow for achieving an equilibrium state. The problem appears to be that there are no excitatory-excitatory weights values that allow a firing rate and energy consumption which can be compensated by the impaired energy production. Specifically, an abrupt change in firing rate due to a small variation in excitatory-excitatory strengths seems to be part of the problem. Thus, small excitatory-excitatory weight variations generate energy consumptions that cannot be compensated by on-demand energy production. This is coherent with the third prediction and shows and extreme case where energy production is so impaired that it is not possible to converge towards a homeostatic balance where energy production and consumption match each other. To understand more intuitively what is happening, besides considering that neurons with impaired metabolism (small K) have slower responses to energy consumptions, thus a higher delay between consumption and production, it is relevant to remember that the excitatory-excitatory weight net drift depends on the available energy in the neurons (see Eqn. (33) and Fig. 5). Thus, if we start the simulation with all the neurons with the homeostatic energy level (*i.e.,* $A(t = 0) = A_H$), given that the energy fixed point value is smaller than the initially available energy (*i.e.,* $\breve{A} < A_H$), then at the begging of the simulation and while the condition $\breve{A} < A(t)$ is fulfilled, weights will increase and, because of the current-rate relationship, firing rates also. Consequently, energy consumption in the neurons increases, but energy production is severely delayed, so the available energy in the neurons will tend to decrease on average (*i.e.,* $\Delta A(t) < 0$). If the available energy continues to decrease, at some point, on average the available energy in the excitatory neurons will be lower than the energy fixed point value (*i.e.,* $A(t) < \breve{A}$). When this condition is fulfilled, the excitatory-excitatory weights will tend to decrease on average, generating a reduction in the excitatory firing rates. This decrease in excitatory-excitatory weights and the accompanying reduction in firing rates will continue while the available energy is lower than the energy fixed point value (*i.e.,* $A(t) < \breve{A}$). This decrease in energy consumption enables the possibility of energy production surpassing the energy consumption (while $\Delta A(t) < 0$ and $A(t) < \breve{A}$ energy

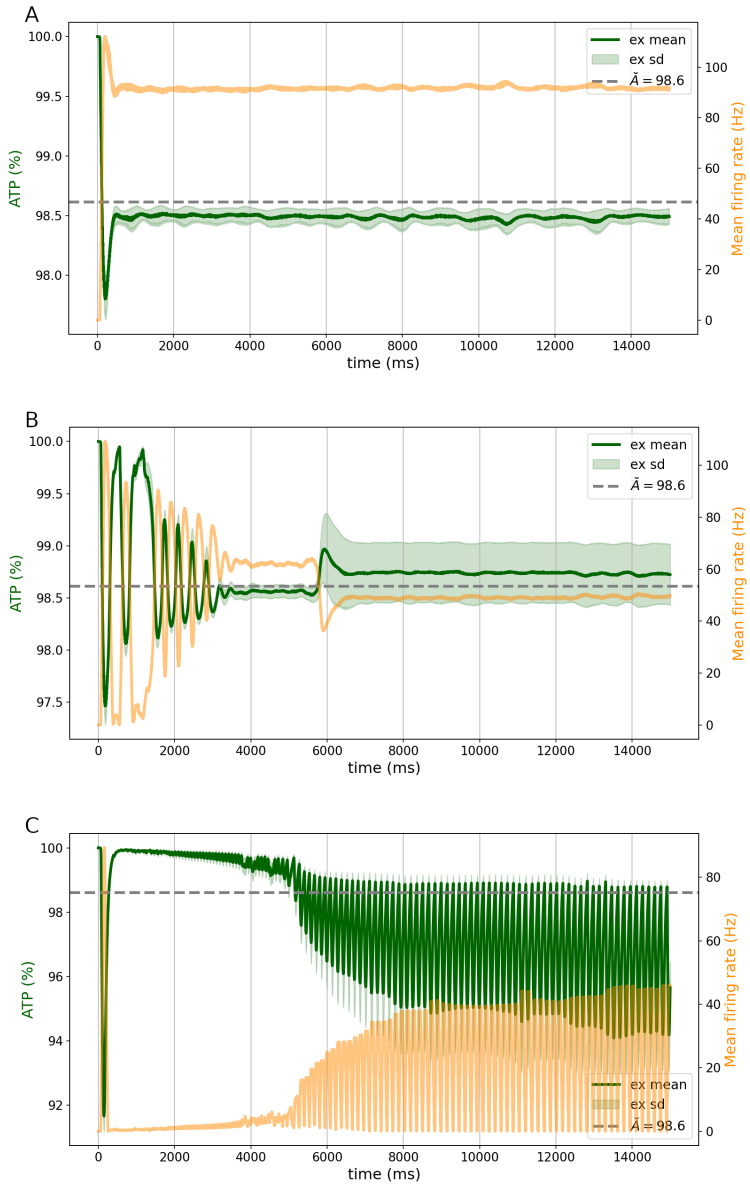

Fig 14. Mean energy and firing rate for different ATP production impairment.
Figure (A) is obtained with $\eta = 50, \gamma = 20, K = 0.7$ parameters, while for Figure (B) $\eta = 50, \gamma = 20, K = 0.5$, and $\eta = 50, \gamma = 20, K = 0.1$ in Figure (C). Figures show the mean energy level and firing rate for the excitatory population.

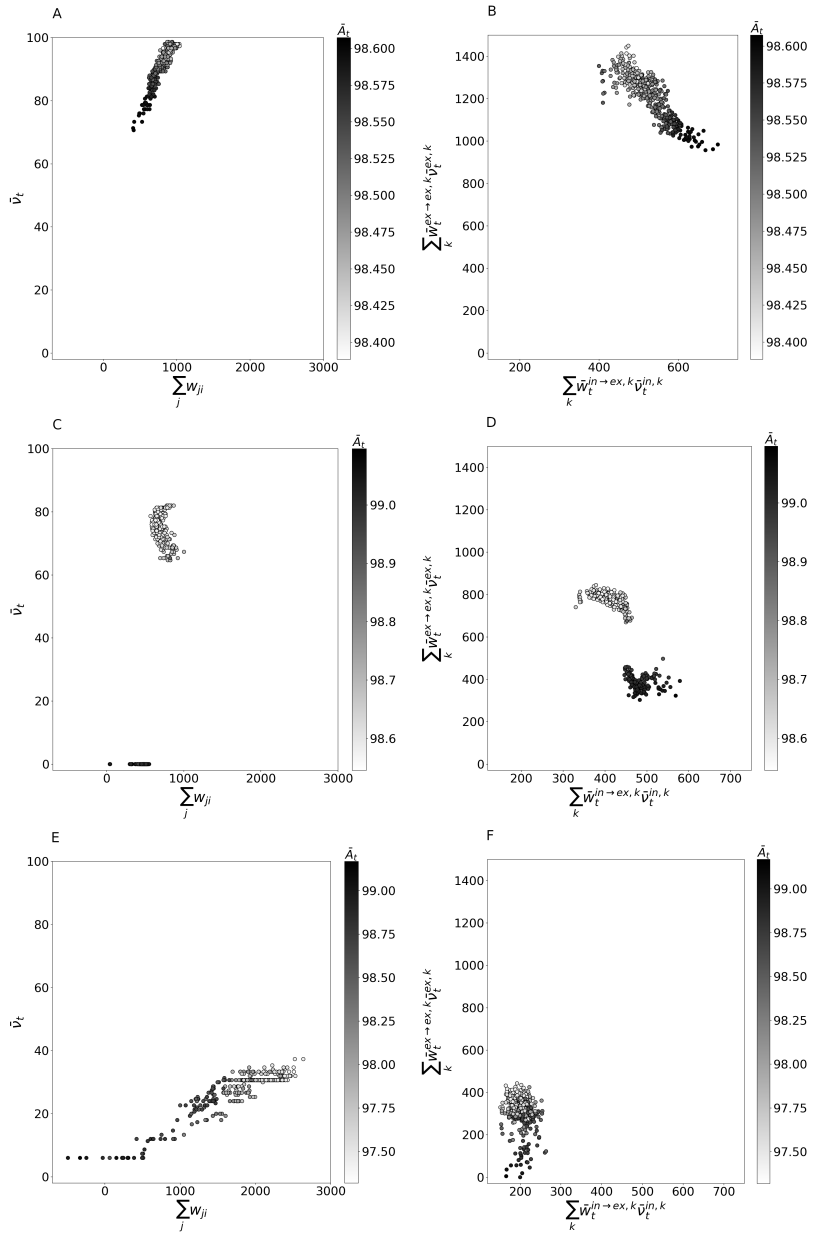

Fig 15. Weight-rate and energy consumption when neuronal ATP production is impaired.
The Figures in the first column show mean firing rates versus incoming synaptic strengths, thus the numerically equivalent to the current-rate mapping defined by $\phi(\cdot)$, while the Figures in the second column show the energy consumption in each neuron due to presynaptic excitatory neurons and presynaptic inhibitory neurons. Figures (A) and (B) are obtained with $\eta = 50, \gamma = 20, K = 0.7$ parameter values, while for Figures (C) and (D) $\eta = 50, \gamma = 20, K = 0.5$. Finally, Figures (E) and (F) show the simulations results when $\eta = 50, \gamma = 20, K = 0.1$. The mean firing rates $\bar{\nu}_t$ in all cases were calculated considering the last 10% of the simulation.

consumption is decreasing but energy production is increasing). If energy production surpasses energy consumption, the available energy in the neurons is increasing (*i.e.,* $\Delta A(t) > 0$). This increase in the available energy $A(t)$ should continue at least until the available energy match the energy equilibrium point (*i.e.,* $A(t) = \breve{A}$), because when the available energy $A(t)$ is below the energy fixed point $\breve{A}$, energy consumption is always decreasing, but energy production is always active (because $A_s(t) = K(A_H - A(t))$). This behavior of energy production and consumption allows that available energy increases above the energy fixed point value $\breve{A}$ in the $\Delta A(t) > 0$ regimen. When the available energy is above the energy $\breve{A}$ equilibrium value, then the loop starts again, and excitatory-excitatory weights as well as excitatory firing rates increase, thus increasing energy consumption faster than the capacity of the neuron to compensate for those consumptions, thus entering the decreasing available energy regimen (*i.e.,* $\Delta A(t) < 0$). This behavior stop when it is possible to match energy production and consumption, while having, on average, available energy near to the energy fixed point (*i.e.,* $A(t) \approx \breve{A}$). When on-demand energy production can compensate for energy consumption in neurons it is easier to find that equilibrium.

Accordingly to our understanding of how energy constraint affects the networks, one possible solution to solve the non-converging system due to a dramatic ATP production impairment ($K = 0.1$), is decreasing the synaptic sensitivity to energy imbalances η. In this manner, synapses experience softer strengths updates transitions when they are close to the analytical fixed-point $\breve{A}$. Thus, diminishing the oscillations due to changes in the peak energy-dependent potentiation described in Eqn. (20). To test this hypothesis, we simulate the network (Fig. 16) with the same initial conditions and parameters as the one shown in Fig. 14C, but decreasing the synaptic sensitivity to energy imbalances to $\eta = 10$. The proposed solution allows for alleviating the oscillations in the system. However, the equilibrium is achieved by silencing a subpopulation of excitatory neurons. The logic behind this phenomenon is the same as the one explained for the $\eta = 50, \gamma = 20, K = 0.5$ case (Figs 14B, 15E and 15F). Fig. 16 shows that non-converging networks due to a dramatic metabolic impairment can be alleviated by modifying other parameters in the network. However, there are other solutions to this problem that might alleviate the oscillations. For instance, a simple solution is to decrease the energy expenditure due to postsynaptic potentials E_{syn}, thus forcing a decrease in energy consumption. Other possible solution could be modifying the neuron's time-constant τ_m. In particular, if τ_m decreases, each neuron has a *slower* dynamic. Thus, decreasing the slope of the current-rate relation. As a consequence, new weights and rates combinations allows to satisfy the required energy constraints, but with lower rates, thus with slower weights updates (weights update when pre- and postsynaptic spikes are present. Thus, lower rates imply less spikes and, therefore, slower weight updates). In addition, if the slope of the current-rate mapping decreases, weights modifications should produce softer transitions in rates, thus helping to decrease the oscillations due to the sensitivity of the firing rates to weights modifications.

Discussion

In this work, inspired by spike-timing-dependent plasticity models, we develop an energy-dependent plasticity model that allows replicating wet-biology experimental results, namely, the suppression of long-term potentiation when the available energy level on the postsynaptic neuron drops [26]. Additionally, we derived a general mathematical expression for the available energy on every neuron in a network with arbitrary architecture.

The energy-dependent STDP model can be interpreted as a neo-Hebbian plasticity rule, where the postsynaptic available energy is driving the change. The newly

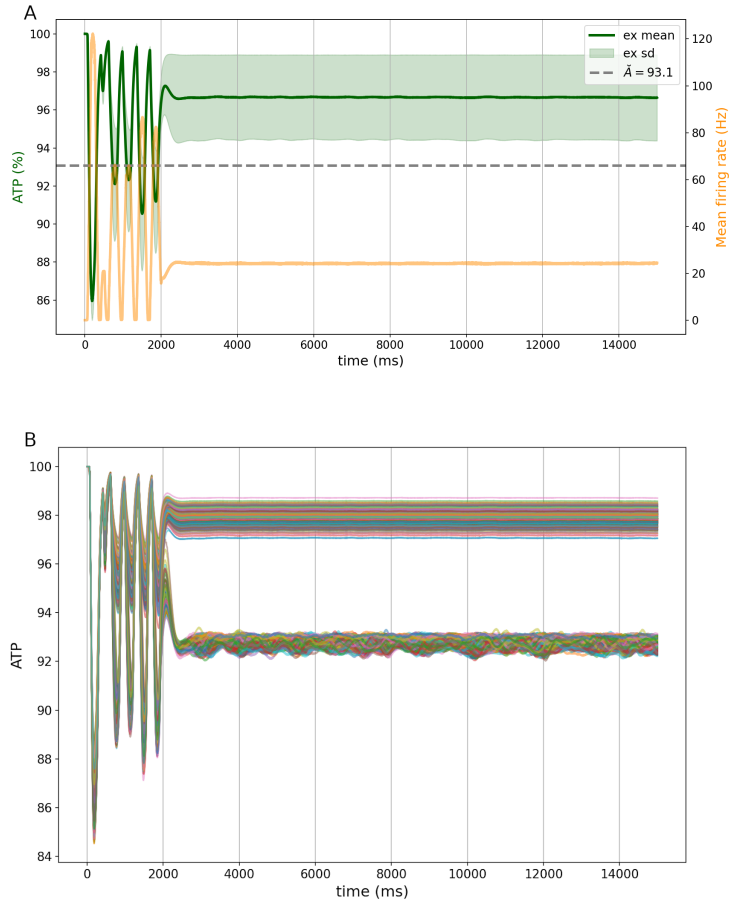

Fig 16. Energy and firing rates for a dramatic metabolic impairment with low synaptic sensitivity to energy imbalances.
Simulations are obtained with $\eta = 10, \gamma = 20, K = 0.1$ parameters. Figures show results for the excitatory population. In particular, (A) shows the mean energy and firing rate dynamics of the entire network, while in (B) the energy dynamic for each neuron in the populations is shown.

introduced model has a general structure that allows the implementation of both, multiplicative and additive learning rules. However, we focus on the additive learning rules (*i.e.,* $\mu_{\pm} = 0$) and found closed-form expression predicting the available energy level equilibrium point $\breve{A}$ on the postsynaptic neuron.

Our model focuses on the effect of postsynaptic available energy on the excitatory-excitatory synaptic potentiation, however, available energy is possibly also affecting depression. The mathematical formulation of ED-STDP (see Eqn. (20)) allows extending of the proposed model for accounting energy dependencies on depression plasticity, and it is part of the future work related to the energy homeostatic principle.

Furthermore, based on the EDLIF model [19] and the ED-STDP plasticity rule introduced in this work, we mathematically formalized and simulated spiking neuronal networks under metabolic constraints. The work focuses on the emergence of dynamics, structure, and the study of attractors under energy constraints for homogeneous neuronal populations in E-I balanced networks. In general terms, the developed theory allows us to predict behaviors observed in numerical experiments. Moreover, the introduced neuronal and synaptic energy constraints generate a new attractor in E-I balanced networks due to the intersection of classic physical constraints (neuronal current-rate relations Eqn. (25)) and the new constraints emerged from the local energy constraint imposed on each neuron in the network. We mathematically describe this phenomenon and conceptualize it in Fig. 7.

Regarding the network's fixed points, synaptic sensitivity to energy imbalances is the main parameter affecting the available energy fixed point for each neuron. As a consequence, through energy-dependent plasticity, synaptic strengths change until non-silent neurons achieve the energy equilibrium point $\breve{A}$. When the weights change, the neurons' firing rates change accordingly. We mathematically describe the required constraints on the postsynaptic neuron between inhibitory and excitatory presynaptic energy consumptions (Eqn. (43)), in order to achieve the energy equilibrium point. Surprisingly, if synaptic sensitivity to energy imbalances η is too high, in order to achieve a global fixed point in the network, the neuronal excitatory population divides into two subpopulations, with one of them composed of silent neurons.

The occurrence of this phenomenon is consistent with biology [34], shedding light on why silencing excitatory neurons could be practical to diminish energy consumption in neuronal networks, thus allowing the network's convergence towards a fixed point. Moreover, this phenomenon can be interpreted as a specialization in the excitatory population. The appearance of a silent subpopulation of neurons is interesting because silent neurons are present in our brains and it is not clear why would we have them. In fact, silent neurons have been referred to as 'dark neurons' in analogy to the astrophysical observation that much of the matter in the universe is undetectable, or dark [34]. In our framework, silent neurons are playing an important role from a metabolic point of view. One hypothesis is that given local energy constraints in biological neural networks, the price to pay due to having redundant neurons in the brain is to silence some of them to achieve a network energy equilibrium.

The effect of neuronal sensitivity to energy imbalances γ in the network's dynamics and structure is also analyzed. Theoretically, the available network's energy fixed point is independent of the neuronal sensitivity to energy imbalances γ. Also, to achieve an energy fixed point when neuronal sensitivity γ is higher, excitatory-excitatory synaptic strengths need to decrease due to higher neuronal excitability produced by increased neuronal sensitivity γ. Numerical experiments confirm the predictions made by theory (Figs 12 and 13).

Regarding neurodegenerative diseases and given the biological evidence suggesting their relation with metabolic impairment, we study how neurons with impaired energy production affect the network dynamics and structure. Our theoretical developments

predict that energy consumption needs to drop in impaired energy production cases. Consequently, lower firing rates and excitatory-excitatory synapses are expected. These predictions are confirmed by numerical experiments (Fig. 15). However, there are other important details in the metabolic impaired scenario. For instance, if the metabolic impairment is high enough, it is also possible that the excitatory population divides into two subpopulations, with one of them composed of silent neurons, although the source of this phenomenon (neuronal incapacity to produce enough energy on demand) is different from the one explained previously when too high synaptic energy sensitivity is present in the network (the energy fixed point $\breve{A}$ must be close to A_H, forcing low energy consumption). Even more dramatic energy production impairments may produce constant oscillations in the network, preventing the convergence toward an attractor (Fig. 14C). We show how these oscillations can be alleviated by modifying other parameters of the simulations. Trying to alleviate the oscillations present in dramatic metabolic impairment scenarios is important because it could help in developing new treatments for neurodegenerative diseases. A detailed study of how to alleviate pathological behaviors due to metabolic impairments is out of the scope of this work. However, the proposed theory as well as the simulation framework could be valuable to deepen the knowledge about the relationship between neurodegenerative diseases and metabolic impairments at the neuronal, synaptic, and network levels.

It is critical to notice that neurodegeneration is usually linked to mitochondrial dysfunction or oxidative stress [35]. Thus, neurodegeneration has been treated by increasing mitochondrial energy production or affecting activity through neurotransmission (e.g., pregabalin to inhibit or levodopa to increase activity). This study proposed an additional avenue for neurodegeneration treatment through synaptic weights. The challenge is to finely regulate energy expenditure and production rather than increase or decrease it in general terms (as currently done). The rationale is that neurons have a mainly aerobic metabolism, with anaerobic activity delegated to astrocytes during increased synaptic activity [14]. Neurons are highly oxidative and selectively low-tolerant to oxidative stress [36]. They maintain a constant expenditure regardless of activity level [37]. Reducing synaptic weight is an important way for a neuron to regulate incoming activity from presynaptic neurons. The synaptic scaling experiments demonstrate this phenomenon by increasing activity by adding a GABAergic inhibitor (Bicuculline) to cultured cortical neurons for long periods (48 hours) [38, 39]. Under this protocol, neurons increase the mean firing rate transiently but later return to a set point value by modulating synaptic weights [40]. This means that exploring potential drugs that boost synaptic weight update velocity may contribute to controlling neurodegenerative processes derived from oxidative stress. Also, our study stresses the need for a better understanding of the fined-tune energy regulation systems in neurons for the development of new therapeutic avenues.

It is important to mention some of the limitations of this work. Firstly, we use a simple single-neuron model that neglects the neuron's morphology and the effect of some relevant ions, such as calcium kinetics, on the neuron's activity. Also, the model includes one type of plasticity, which only modifies excitatory-excitatory connections. Thus, we are neglecting other types of plasticity acting at different time scales, such as short-term plasticity or synaptic scaling. In addition, all the connections in the model, except excitatory-excitatory connections, are static. This is also an important limitation because different types of plasticity acting on other connections could have a significant impact on the network's activity and structure.

In general, previous neuronal and synaptic models do not account for energy dependencies. Thus, the developed framework, analysis of dynamics, and structure in spiking neural networks under metabolic impairment as well as the analysis of the effect of energy constraints in E-I balanced networks are the main contributions of this work.

Regarding future work, there are a few avenues along which to continue and extend the work presented here. Firstly, while our focus was on integrating energy-dependent long-term plasticity within excitatory-excitatory connections, other connection types could similarly undergo energy-dependent plastic alterations, warranting broader model inclusion. Additionally, our emphasis on long-term synaptic modifications might benefit from an expanded scope that captures plasticity across diverse temporal scales. For instance, incorporating short-term plasticity rules, especially with insights from established models such us the formalization introduced [41], could offer a richer understanding of synaptic dynamics, particularly when energy dependencies in processes like synaptic vesicle recycling are considered [8, 9]. Moreover, our study's homogeneous approach, which presumed uniform neuron parameters, might be broadened to encompass the inherent variability of biological systems by investigating heterogeneous neural network under metabolic constraints. Lastly, a more detailed exploration into the coupling phenomena among neurons, given our plasticity mechanism's reliance on spike timings, could shed light on its structural implications for networks. This would involve both analytical studies and simulations to discern the overarching effects on network architecture and function.

Acknowledgments

This work has been partially supported by National Center for Artificial Intelligence CENIA FB210017, FONDECYT 1210031, Advanced Center for Electrical and Electronic Engineering, Basal Project FB0008, and Basal ANID given to P.M. and R.C.V. The authors also wish to thank ANID-PFCHA/Doctorado Nacional/2019-21190330 for supporting Ismael Jaras' doctoral studies.

References

1. Shulman RG, Rothman DL, Behar KL, Hyder F. Energetic basis of brain activity: implications for neuroimaging. Trends in Neurosciences. 2004;27(8):489–495. doi:10.1016/j.tins.2004.06.005.

2. Harris JJ, Jolivet R, Attwell D. Synaptic Energy Use and Supply. Neuron. 2012;75(5):762 – 777. doi:https://doi.org/10.1016/j.neuron.2012.08.019.

3. Ames A. CNS energy metabolism as related to function. Brain Research Reviews. 2000;34(1):42 – 68. doi:https://doi.org/10.1016/S0165-0173(00)00038-2.

4. Lin MT, Beal MF. Mitochondrial dysfunction and oxidative stress in neurodegenerative diseases. Nature. 2006;443(7113):787–795. doi:10.1038/nature05292.

5. Kawamata H, Manfredi G. Mitochondrial dysfunction and intracellular calcium dysregulation in ALS. Mechanisms of Ageing and Development. 2010;131(7):517 – 526. doi:https://doi.org/10.1016/j.mad.2010.05.003.

6. Maruszak A, Żekanowski C. Mitochondrial dysfunction and Alzheimer's disease. Progress in Neuro-Psychopharmacology and Biological Psychiatry. 2011;35(2):320 – 330. doi:https://doi.org/10.1016/j.pnpbp.2010.07.004.

7. Park JS, Davis RL, Sue CM. Mitochondrial Dysfunction in Parkinson's Disease: New Mechanistic Insights and Therapeutic Perspectives. Current neurology and neuroscience reports. 2018;18(5):21–21. doi:10.1007/s11910-018-0829-3.

8. Pathak D, Shields LY, Mendelsohn BA, Haddad D, Lin W, Gerencser AA, et al. The Role of Mitochondrially Derived ATP in Synaptic Vesicle Recycling. Journal of Biological Chemistry. 2015;290(37):22325–22336. doi:10.1074/jbc.M115.656405.

9. Rangaraju V, Calloway N, Ryan TA. Activity-Driven Local ATP Synthesis Is Required for Synaptic Function. Cell. 2014;156(4):825–835. doi:10.1016/j.cell.2013.12.042.

10. Vergara RC, Jaramillo-Riveri S, Luarte A, Moënne-Loccoz C, Fuentes R, Couve A, et al. The Energy Homeostasis Principle: Neuronal Energy Regulation Drives Local Network Dynamics Generating Behavior. Frontiers in Computational Neuroscience. 2019;13:49. doi:10.3389/fncom.2019.00049.

11. Vicencio-Jimenez S, Villalobos M, Maldonado PE, Vergara RC. The Energy Homeostasis Principle: A Naturalistic Approach to Explain the Emergence of Behavior. Frontiers in Systems Neuroscience. 2022;15. doi:10.3389/fnsys.2021.782781.

12. Sokoloff L. The physiological and biochemical bases of functional brain imaging. Cognitive Neurodynamics. 2007;2(1):1–5. doi:10.1007/s11571-007-9033-x.

13. Schulz K, Sydekum E, Krueppel R, Engelbrecht CJ, Schlegel F, Schröter A, et al. Simultaneous BOLD fMRI and fiber-optic calcium recording in rat neocortex. Nature Methods. 2012;9(6):597–602. doi:10.1038/nmeth.2013.

14. Weber B, Barros LF. The Astrocyte: Powerhouse and Recycling Center. Cold Spring Harbor Perspectives in Biology. 2015; p. a020396. doi:10.1101/cshperspect.a020396.

15. Connolly NMC, Dussmann H, Anilkumar U, Huber HJ, Prehn JHM. Single-Cell Imaging of Bioenergetic Responses to Neuronal Excitotoxicity and Oxygen and Glucose Deprivation. Journal of Neuroscience. 2014;34(31):10192–10205. doi:10.1523/jneurosci.3127-13.2014.

16. Jekabsons MB, Nicholls DG. In Situ Respiration and Bioenergetic Status of Mitochondria in Primary Cerebellar Granule Neuronal Cultures Exposed Continuously to Glutamate. Journal of Biological Chemistry. 2004;279(31):32989–33000. doi:10.1074/jbc.m401540200.

17. Lange SC, Winkler U, Andresen L, Byhrø M, Waagepetersen HS, Hirrlinger J, et al. Dynamic Changes in Cytosolic ATP Levels in Cultured Glutamatergic Neurons During NMDA-Induced Synaptic Activity Supported by Glucose or Lactate. Neurochemical Research. 2015;40(12):2517–2526. doi:10.1007/s11064-015-1651-9.

18. Toloe J, Mollajew R, Kügler S, Mironov SL. Metabolic differences in hippocampal 'Rett' neurons revealed by ATP imaging. Molecular and Cellular Neuroscience. 2014;59:47–56. doi:10.1016/j.mcn.2013.12.008.

19. Jaras I, Harada T, Orchard ME, Maldonado PE, Vergara RC. Extending the integrate-and-fire model to account for metabolic dependencies. European Journal of Neuroscience. 2021;54(4):5249–5260. doi:https://doi.org/10.1111/ejn.15326.

20. LeMasson G, Przedborski S, Abbott LF. A Computational Model of Motor Neuron Degeneration. Neuron. 2014;83(4):990. doi:10.1016/j.neuron.2014.08.018.

21. Bugmann G, Christodoulou C, Taylor JG. Role of Temporal Integration and Fluctuation Detection in the Highly Irregular Firing of a Leaky Integrator Neuron Model with Partial Reset. Neural Computation. 1997;9:985–1000.

22. Burkitt AN. A Review of the Integrate-and-fire Neuron Model: I. Homogeneous Synaptic Input. Biological Cybernetics. 2006;95(1):1–19. doi:10.1007/s00422-006-0068-6.

23. Elisabeth E, David A. Non-signalling energy use in the brain. The Journal of Physiology. 2015;593(16):3417–3429. doi:10.1113/jphysiol.2014.282517.

24. Todorova V, Blokland A. Mitochondria and Synaptic Plasticity in the Mature and Aging Nervous System. Current neuropharmacology. 2017;15(1):166–173. doi:10.2174/1570159X14666160414111821.

25. Gütig R, Aharonov R, Rotter S, Sompolinsky H. Learning Input Correlations through Nonlinear Temporally Asymmetric Hebbian Plasticity. Journal of Neuroscience. 2003;23(9):3697–3714. doi:10.1523/JNEUROSCI.23-09-03697.2003.

26. Potter WB, O'Riordan KJ, Barnett D, Osting SMK, Wagoner M, Burger C, et al. Metabolic Regulation of Neuronal Plasticity by the Energy Sensor AMPK. PLOS ONE. 2010;5(2):1–9. doi:10.1371/journal.pone.0008996.

27. Wang Y, Shi X, Si B, Cheng B, Chen J. Synchronization and oscillation behaviors of excitatory and inhibitory populations with spike-timing-dependent plasticity. Cognitive Neurodynamics. 2022;doi:10.1007/s11571-022-09840-z.

28. Bi Gq, Poo Mm. Synaptic Modifications in Cultured Hippocampal Neurons: Dependence on Spike Timing, Synaptic Strength, and Postsynaptic Cell Type. Journal of Neuroscience. 1998;18(24):10464–10472. doi:10.1523/JNEUROSCI.18-24-10464.1998.

29. Gewaltig MO, Diesmann M. NEST (NEural Simulation Tool). Scholarpedia. 2007;2(4):1430.

30. Linssen CAP, Babu PN, Benelhedi A, De Schepper R, Fardet T, Eppler JM, et al.. NESTML 5.0.0; 2022. Available from: `https://doi.org/10.5281/zenodo.5784175`.

31. Sahara S, Yanagawa Y, O'Leary DDM, Stevens CF. The Fraction of Cortical GABAergic Neurons Is Constant from Near the Start of Cortical Neurogenesis to Adulthood. Journal of Neuroscience. 2012;32(14):4755–4761. doi:10.1523/JNEUROSCI.6412-11.2012.

32. Bettencourt LMA, Stephens GJ, Ham MI, Gross GW. Functional structure of cortical neuronal networks grown in vitro. Phys Rev E. 2007;75:021915. doi:10.1103/PhysRevE.75.021915.

33. Kempter R, Gerstner W, van Hemmen JL. Hebbian learning and spiking neurons. Phys Rev E. 1999;59:4498–4514. doi:10.1103/PhysRevE.59.4498.

34. Shoham S, O'Connor DH, Segev R. How silent is the brain: is there a "dark matter" problem in neuroscience? Journal of Comparative Physiology A. 2006;192(8):777–784. doi:10.1007/s00359-006-0117-6.

35. Cenini G, Lloret A, Cascella R. Oxidative Stress in Neurodegenerative Diseases: From a Mitochondrial Point of View. Oxidative Medicine and Cellular Longevity. 2019;2019:1–18. doi:10.1155/2019/2105607.

36. Wang. Selective neuronal vulnerability to oxidative stress in the brain. Frontiers in Aging Neuroscience. 2010;doi:10.3389/fnagi.2010.00012.

37. Baeza-Lehnert F, Saab AS, Gutiérrez R, Larenas V, Díaz E, Horn M, et al. Non-Canonical Control of Neuronal Energy Status by the Na^+ Pump. Cell Metabolism. 2019;29(3):668–680.e4. doi:10.1016/j.cmet.2018.11.005.

38. Turrigiano GG. The Self-Tuning Neuron: Synaptic Scaling of Excitatory Synapses. Cell. 2008;135(3):422–435. doi:10.1016/j.cell.2008.10.008.

39. Turrigiano G. Homeostatic Synaptic Plasticity: Local and Global Mechanisms for Stabilizing Neuronal Function. Cold Spring Harbor Perspectives in Biology. 2011;4(1):a005736–a005736. doi:10.1101/cshperspect.a005736.

40. Ibata K, Sun Q, Turrigiano GG. Rapid Synaptic Scaling Induced by Changes in Postsynaptic Firing. Neuron. 2008;57(6):819–826. doi:10.1016/j.neuron.2008.02.031.

41. Tsodyks MV, Markram H. The neural code between neocortical pyramidal neurons depends on neurotransmitter release probability. Proceedings of the National Academy of Sciences. 1997;94(2):719–723. doi:10.1073/pnas.94.2.719.

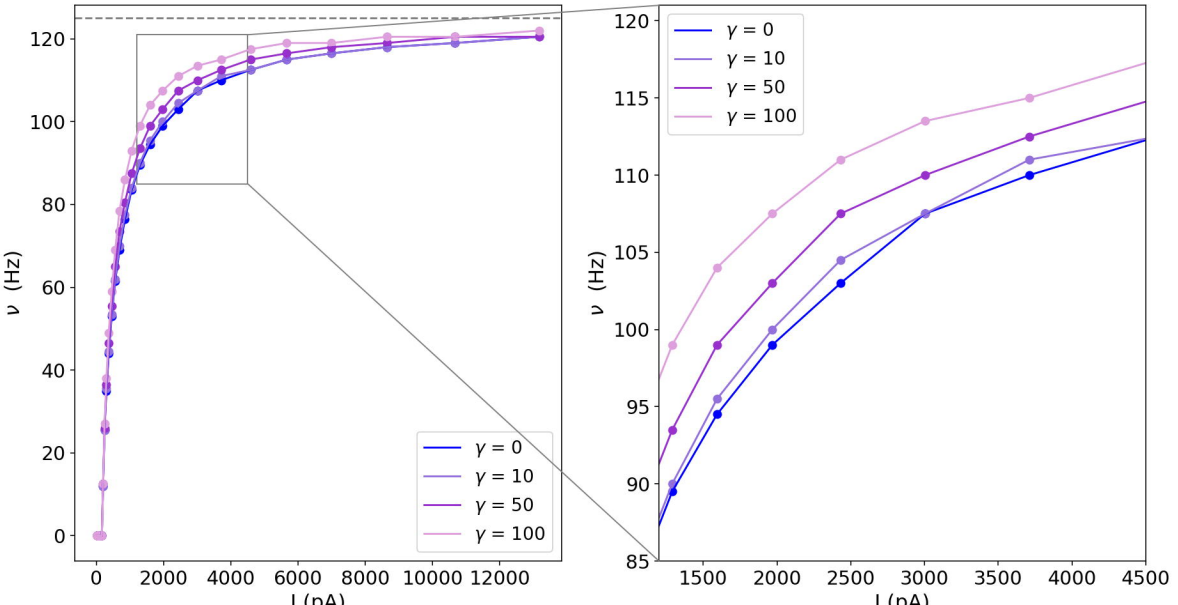
ν (Hz)
I (pA)
γ = 0
γ = 10
γ = 50
γ = 100
0
20
40
60
80
100
120
0
2000
4000
6000
8000
10000
12000
85
90
95
100
105
110
115
120
1500
2000
2500
3000
3500
4000
4500

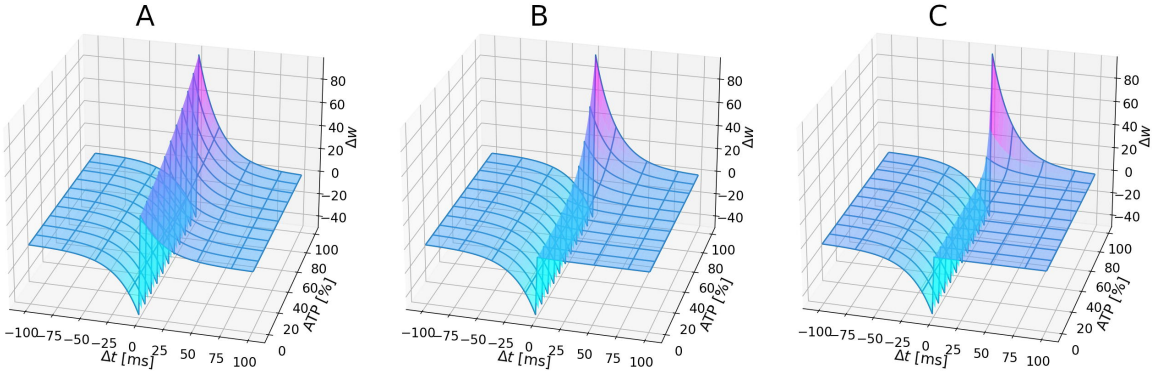
A
B
C
Δw
ATP [%]
Δt [ms]
80
60
40
20
0
−20
−40
100
80
60
40
20
0
−100
−75
−50
−25
0
25
50
75
100

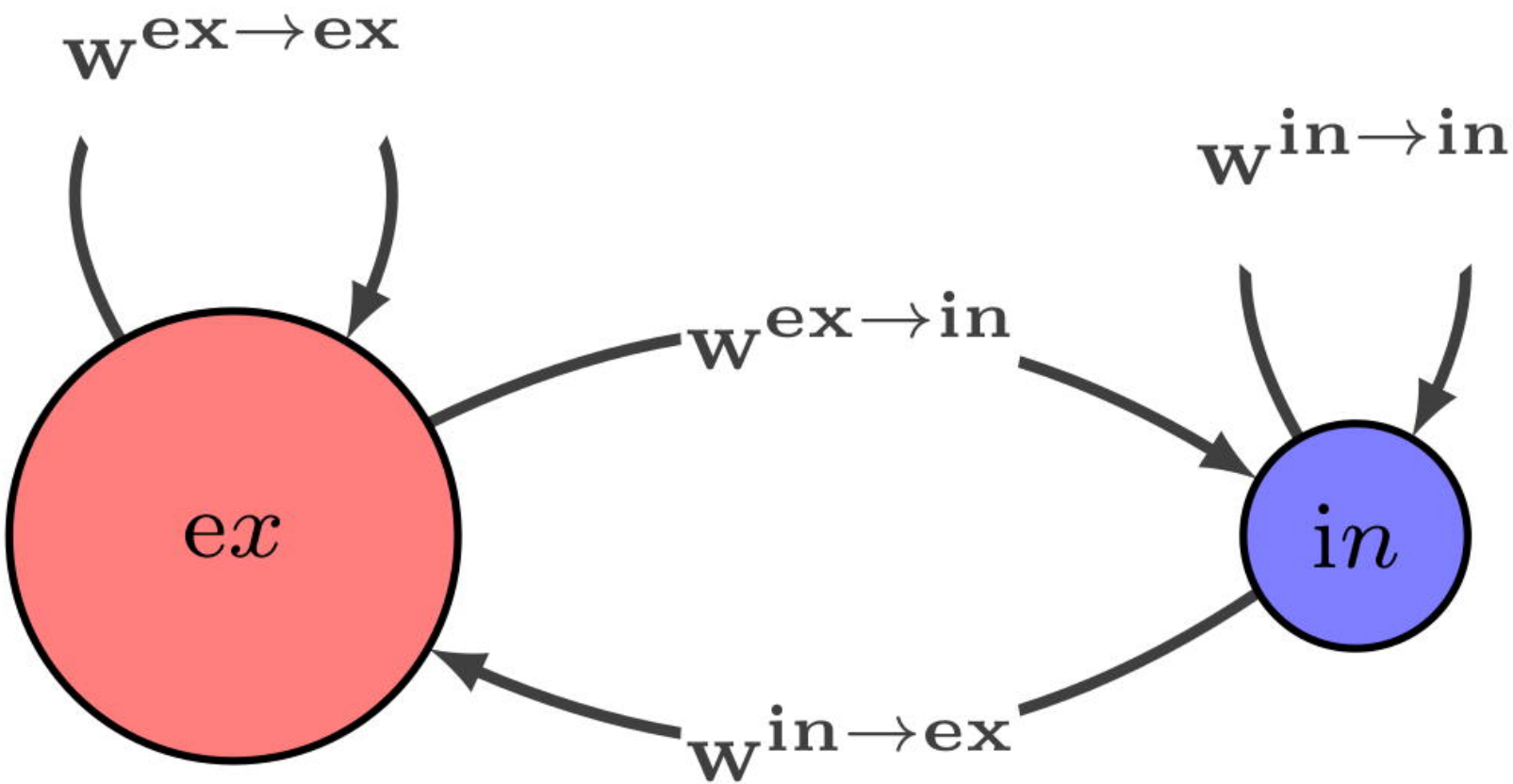
$\mathbf{w}^{\mathbf{ex}\to\mathbf{ex}}$
$\mathbf{w}^{\mathbf{in}\to\mathbf{in}}$
$\mathbf{w}^{\mathbf{ex}\to\mathbf{in}}$
ex
in
$\mathbf{w}^{\mathbf{in}\to\mathbf{ex}}$

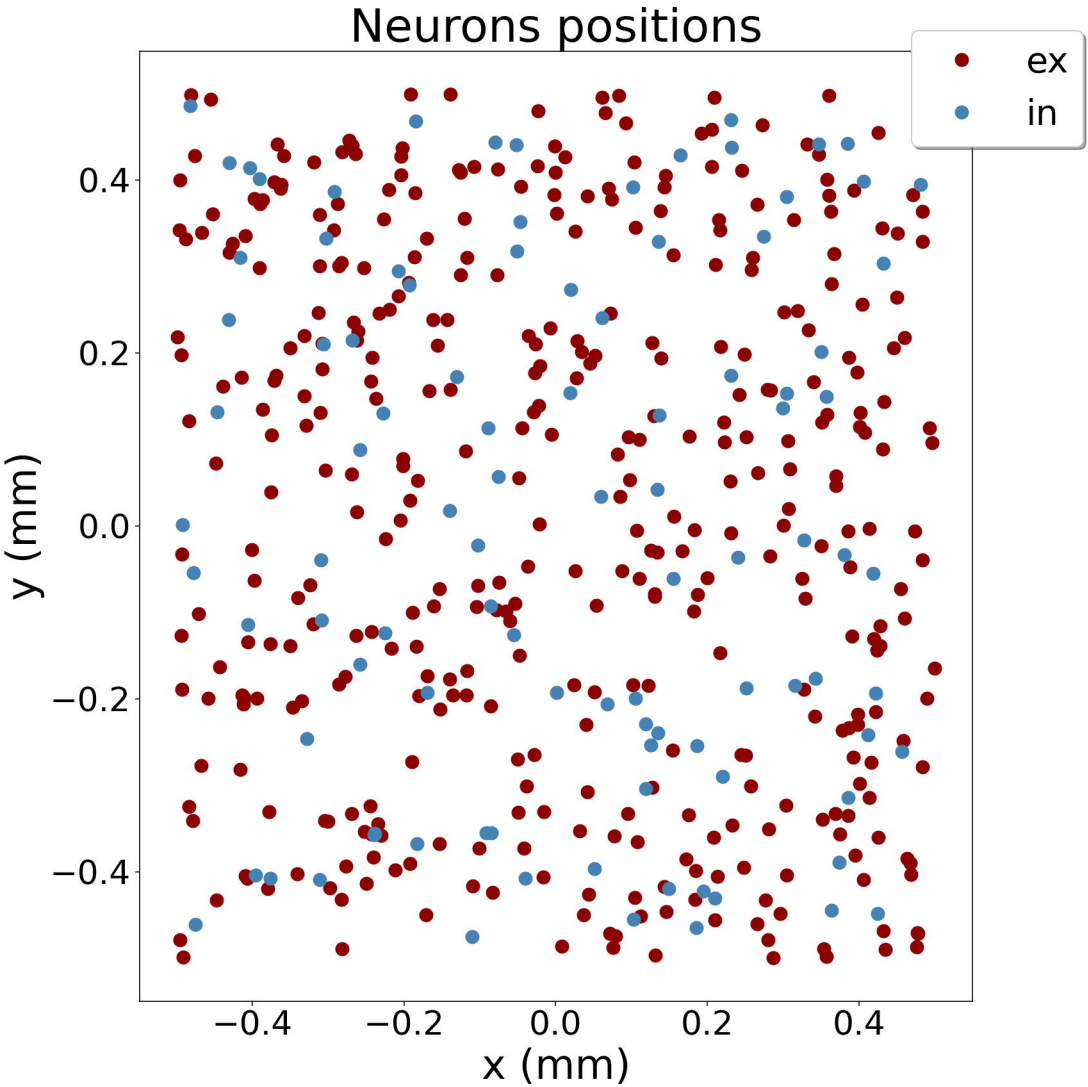
Neurons positions
ex
in
0.4
0.2
0.0
−0.2
−0.4
y (mm)
−0.4
−0.2
0.0
0.2
0.4
x (mm)

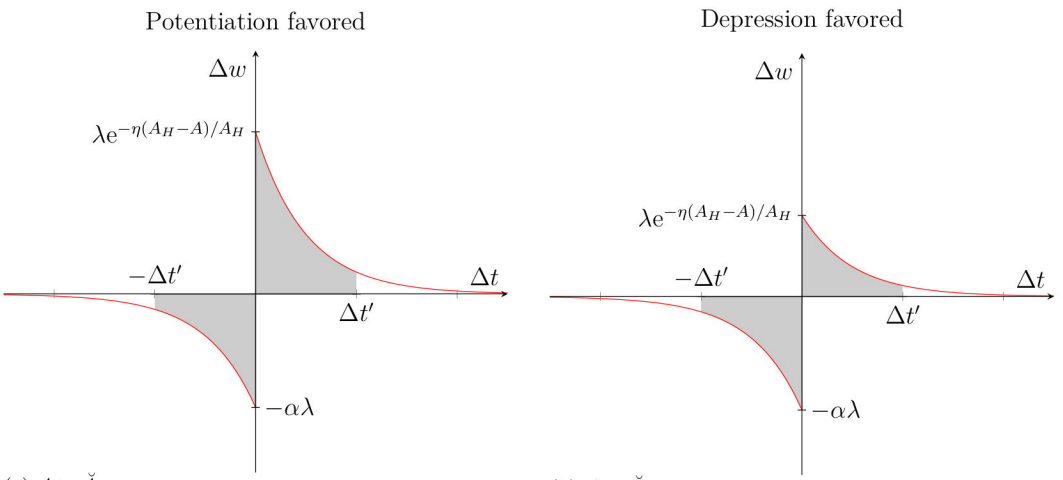

(a) $A > \breve{A}$

(b) $A < \breve{A}$

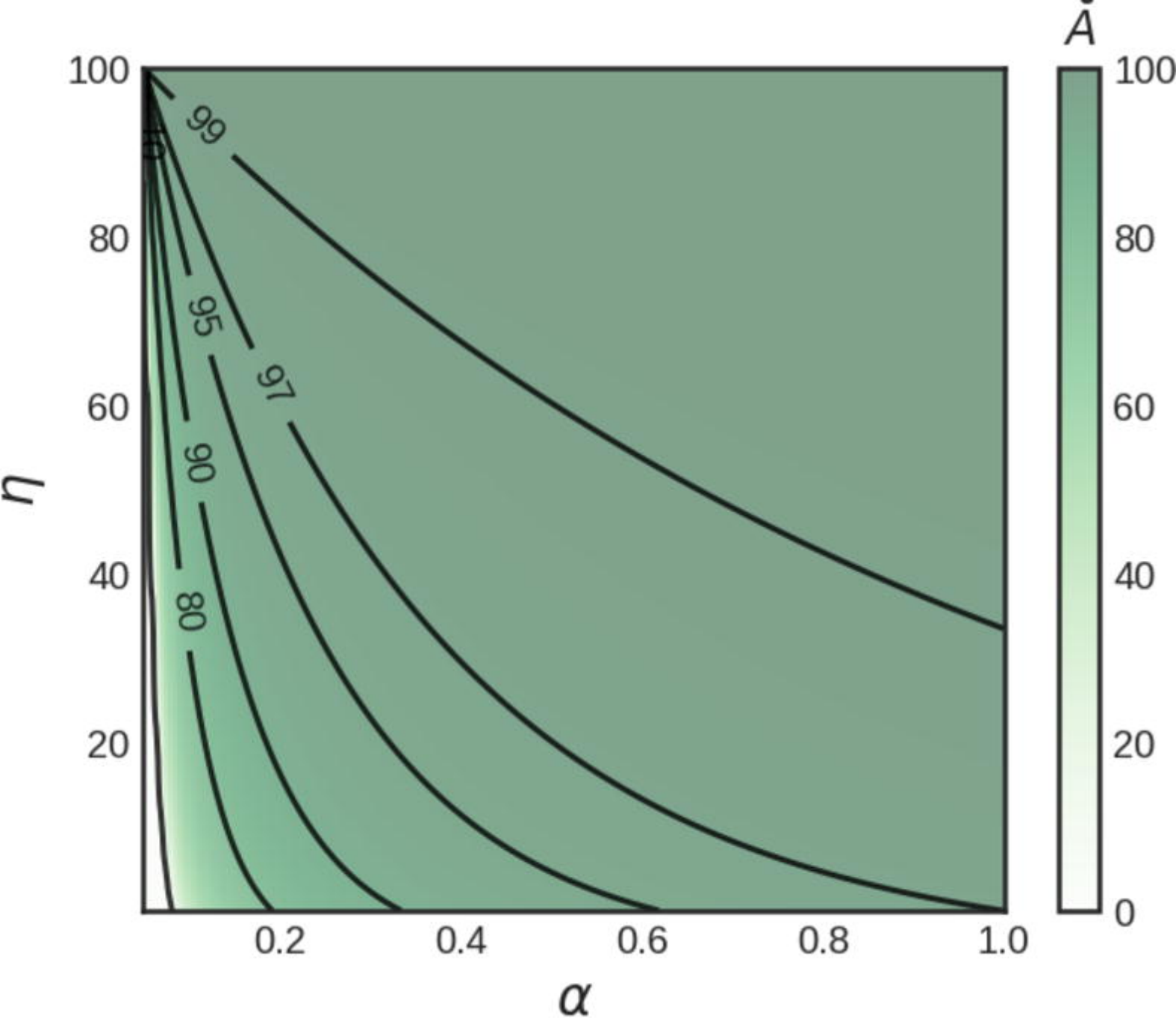
$\dot{A}$
100
80
60
40
20
0
99
95
97
90
80
η
0.2
0.4
0.6
0.8
1.0
α

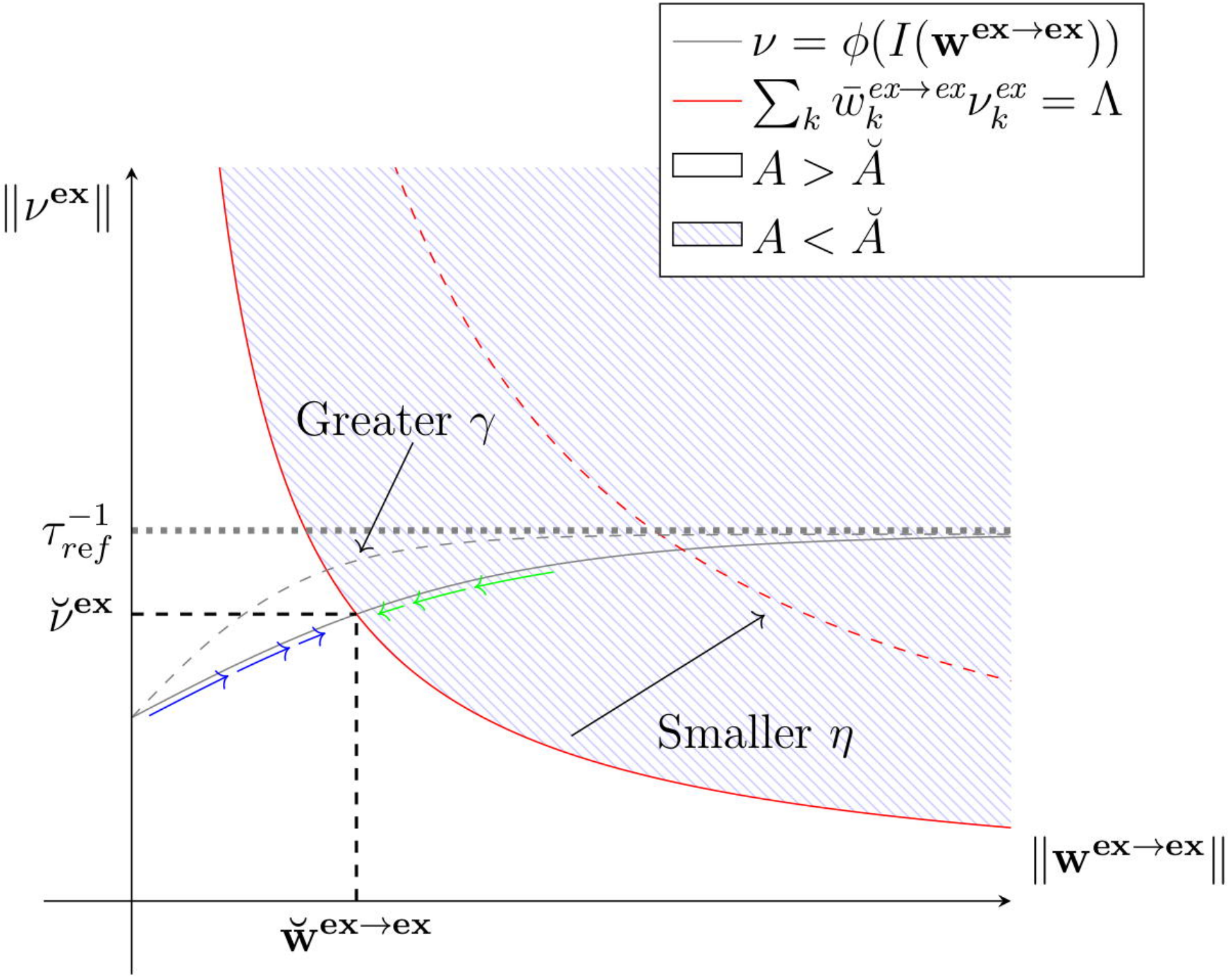
$\nu = \phi(I(\mathbf{w}^{\mathbf{ex}\to\mathbf{ex}}))$
$\sum_k \bar{w}_k^{ex\to ex}\nu_k^{ex} = \Lambda$
$A > \breve{A}$
$A < \breve{A}$
$\|\nu^{\mathbf{ex}}\|$
Greater γ
τ_{ref}^{-1}
$\breve{\nu}^{\mathbf{ex}}$
Smaller η
$\|\mathbf{w}^{\mathbf{ex}\to\mathbf{ex}}\|$
$\breve{\mathbf{w}}^{\mathbf{ex}\to\mathbf{ex}}$

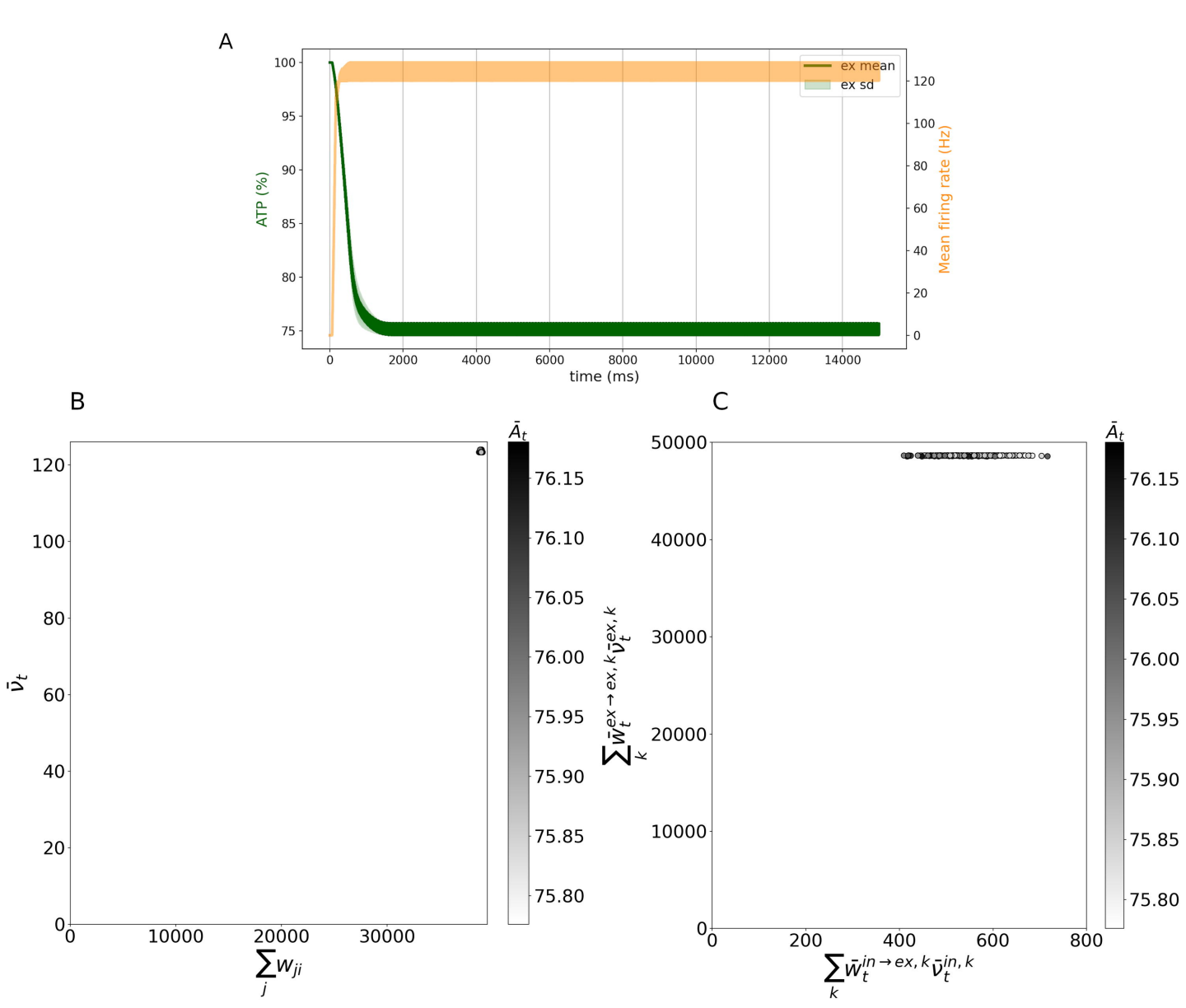
A
ex mean
ex sd
ATP (%)
Mean firing rate (Hz)
time (ms)
B
$\bar{\nu}_t$
$\sum_j w_{ji}$
$\bar{A}_t$
C
$\sum_k \bar{w}_t^{ex \to ex,k} \bar{\nu}_t^{ex,k}$
$\sum_k \bar{w}_t^{in \to ex,k} \bar{\nu}_t^{in,k}$
$\bar{A}_t$

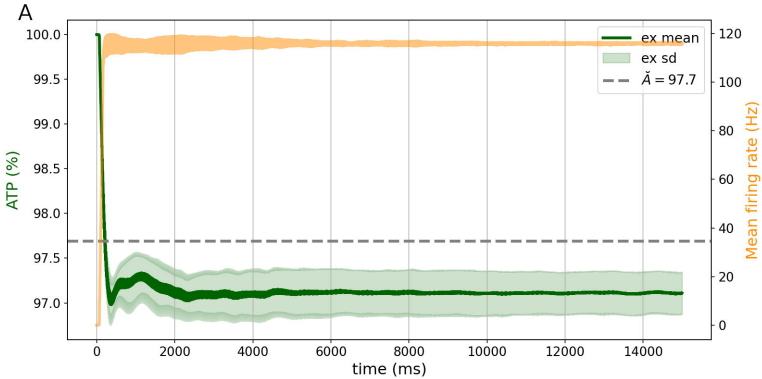
A
ex mean
ex sd
$\check{A} = 97.7$
ATP (%)
Mean firing rate (Hz)
time (ms)

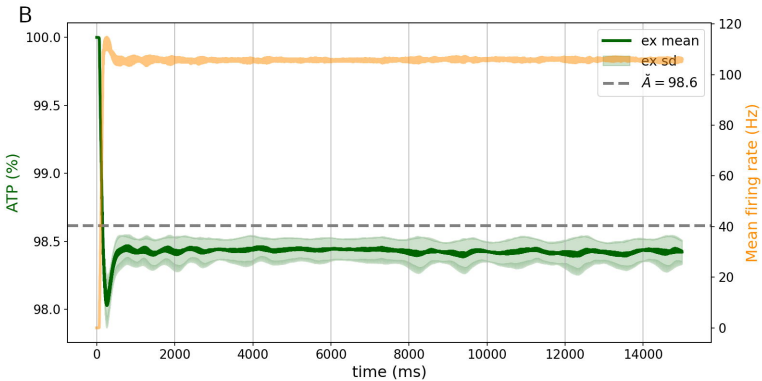
B
ex mean
ex sd
$\check{A} = 98.6$
ATP (%)
Mean firing rate (Hz)
time (ms)

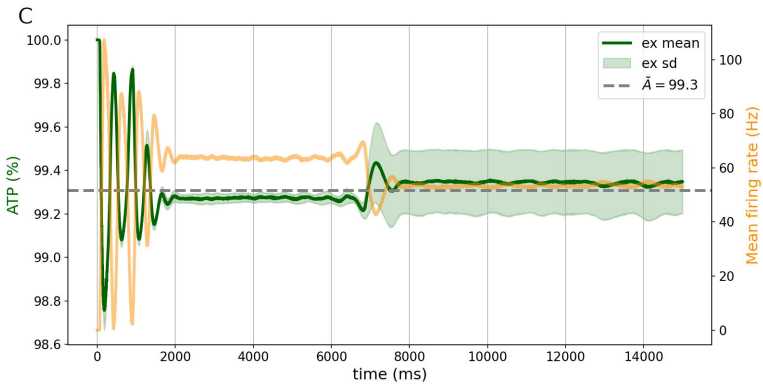
C
ex mean
ex sd
$\check{A} = 99.3$
ATP (%)
Mean firing rate (Hz)
time (ms)

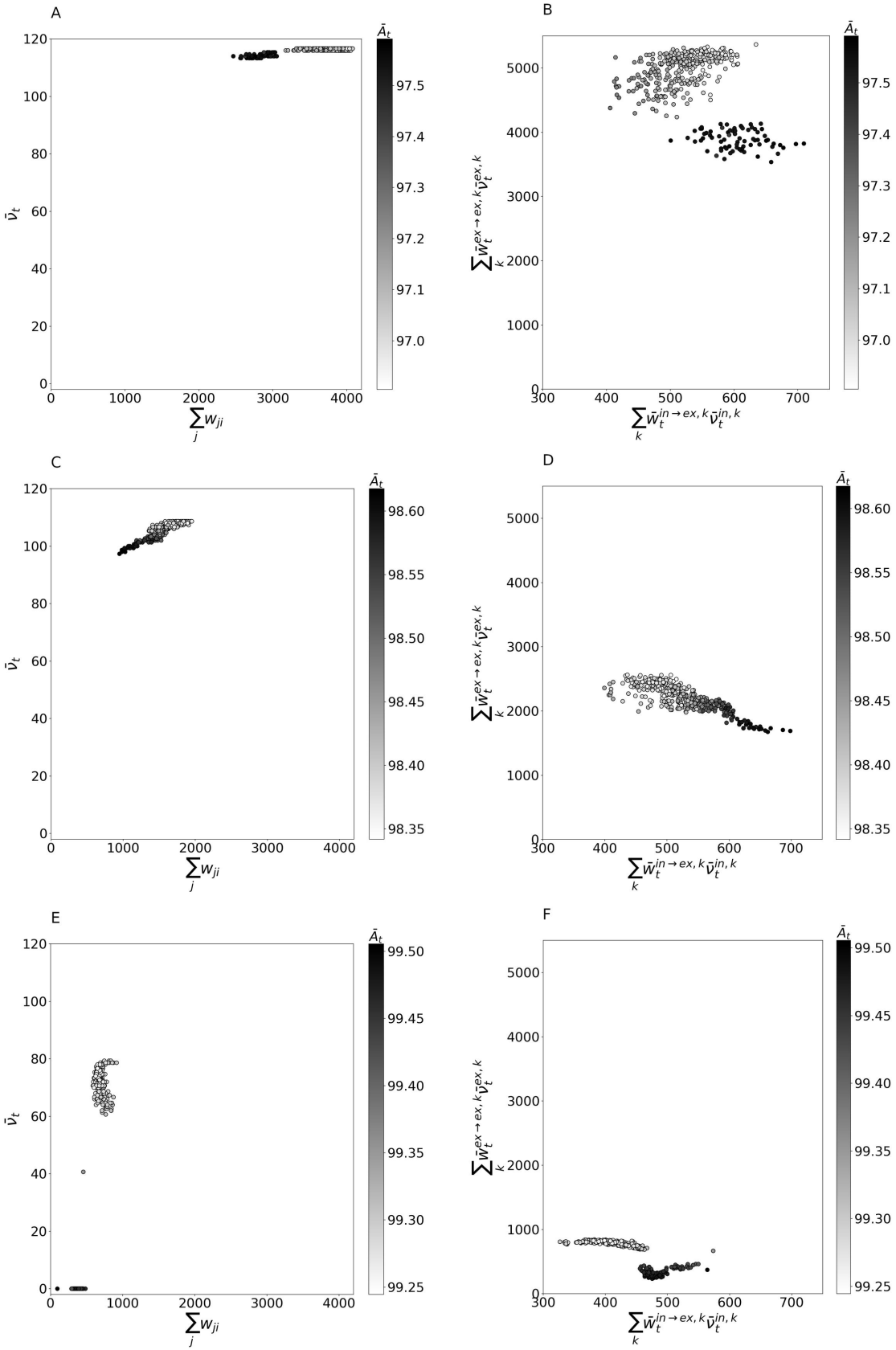
A
B
C
D
E
F
$\bar{A}_t$
$\bar{\nu}_t$
$\sum_j w_{ji}$
$\sum_k \bar{w}_t^{ex \to ex,k} \bar{\nu}_t^{ex,k}$
$\sum_k \bar{w}_t^{in \to ex,k} \bar{\nu}_t^{in,k}$

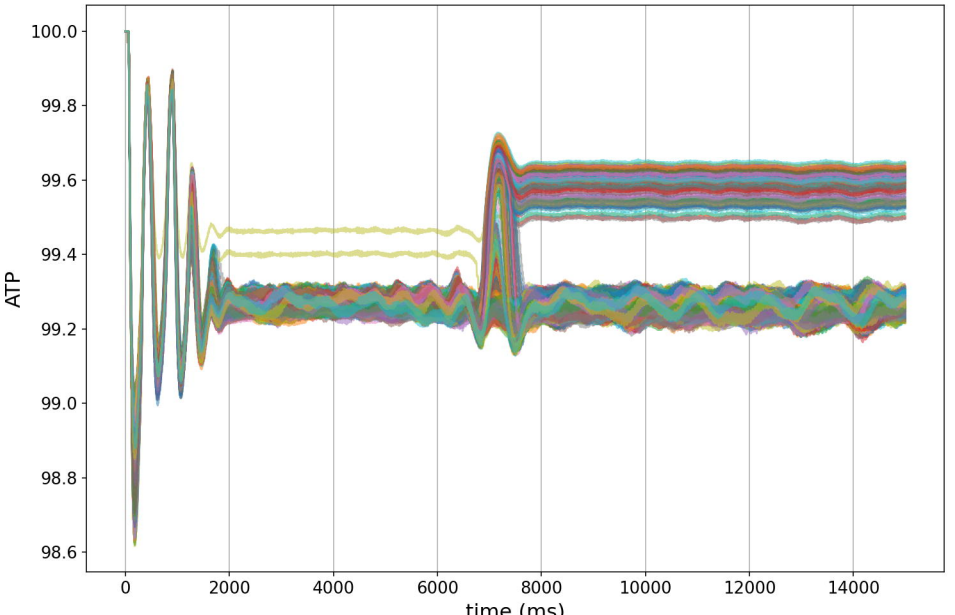
100.0
99.8
99.6
99.4
99.2
99.0
98.8
98.6
ATP
0
2000
4000
6000
8000
10000
12000
14000
time (ms)

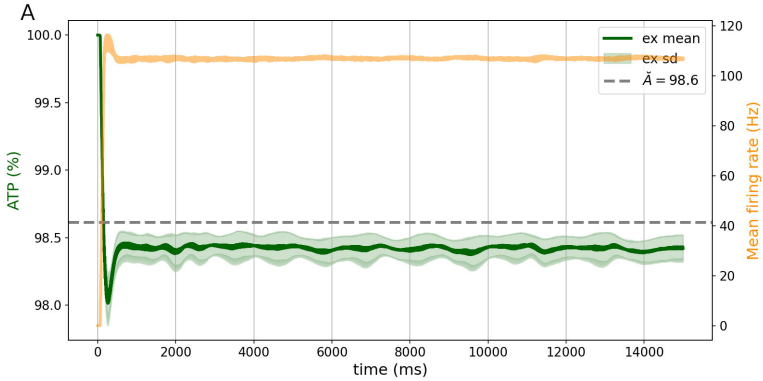
A
ex mean
ex sd
$\check{A} = 98.6$
ATP (%)
Mean firing rate (Hz)
time (ms)

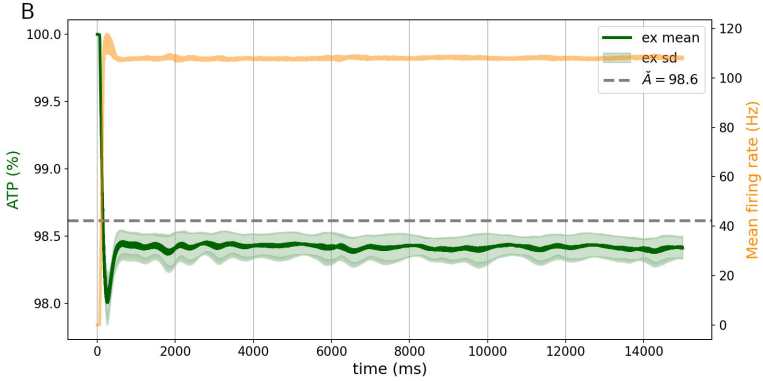
B
ex mean
ex sd
$\check{A} = 98.6$
ATP (%)
Mean firing rate (Hz)
time (ms)

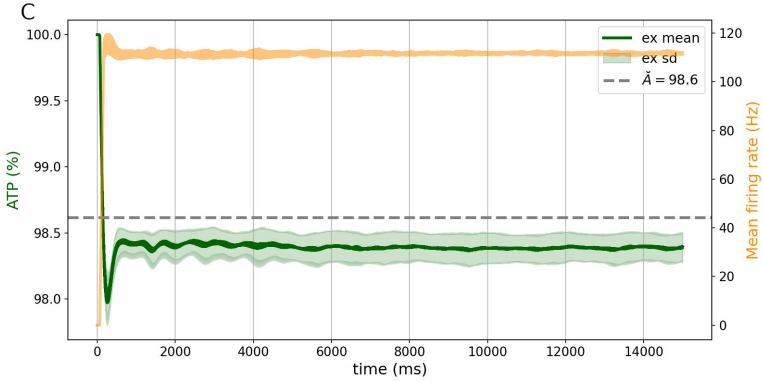
C
ex mean
ex sd
$\check{A} = 98.6$
ATP (%)
Mean firing rate (Hz)
time (ms)